

We are IntechOpen, the world's leading publisher of Open Access books Built by scientists, for scientists

6,900

Open access books available

186,000

International authors and editors

200M

Downloads

Our authors are among the

154

Countries delivered to

TOP 1%

most cited scientists

12.2%

Contributors from top 500 universities



WEB OF SCIENCE™

Selection of our books indexed in the Book Citation Index
in Web of Science™ Core Collection (BKCI)

Interested in publishing with us?
Contact book.department@intechopen.com

Numbers displayed above are based on latest data collected.
For more information visit www.intechopen.com



Advanced Sensor and Dynamics Models with an Application to Sensor Management

Wolfgang Koch

German Defence Research Establishment (FGAN e.V.)

Germany

1. Introduction

The methods provided by sensor and data fusion [14] are important tools for fusing large sets of mutually complementary data and efficiently exploiting the sensor systems available. A challenging exploitation technology at the common interface between sensors, command & control systems, and the human decision makers involved, this technology plays a key role in applications with time-critical situations or in situations with a high decision risk, where human deficiencies are to be compensated by automatically or interactively working fusion techniques (compensating decreasing attention in routine situations, focusing the attention on anomalous or rare events, complementing limited memory, reaction, or combination capabilities of human beings). Besides the advantages of reducing the human work load in routine or mass tasks, data fusion from mutually complementary information sources can well produce qualitatively new knowledge that otherwise would remain unrevealed.

A. Providing Elements for Situation Pictures

Sensor and data fusion provides 'information elements' for producing near real-time situation pictures, which electronically represent a complex and dynamically evolving overall scenario in the air, on the ground, at sea, or in an urban environment. The concrete operational requirements in a given application define the particular information sources to be fused. A careful analysis of the underlying requirements is thus essential for any fusion system design.

Information elements are extracted from currently received sensor data while taking into account the available context knowledge and pre-history. They typically provide answers to questions related to objects of interest such as: Do objects exist at all, and how many of them are in the sensors' fields of view? Where are they at what time? Where will they be in the future with what probability? How can their overall behavior be characterized? Are anomalies or hints about their possible intentions recognizable? What can be inferred about the classes the objects belong to or even their identities? Are there characteristic interrelations between individual objects? In which regions do they have their origin? What can be said about their possible destinations? Are object flows visible? Where are sources or sinks of traffic?

The sensor data to be fused can be inaccurate, incomplete, or ambiguous. Closely-spaced objects are often totally or partially unresolvable. Possibly, the measured object parameters

Source: Sensor and Data Fusion, Book edited by: Dr. ir. Nada Milisavljević,
ISBN 978-3-902613-52-3, pp. 490, February 2009, I-Tech, Vienna, Austria

are false or corrupted by hostile measures. The context information is in many cases hard to be formalized or even contradictory. These deficiencies of the information to be fused are unavoidable in any real-world application. Therefore, the extraction of 'information elements' for situation pictures is by no means trivial.

B. Aspects of Sensor and Data Fusion

Among the primary technical prerequisites for sensor data and information fusion are communication links with a sufficient bandwidth, small latency, and robustness against failure or jamming. Moreover, the transformation of the sensor data into a common coordinate system requires a precise space-time registration of the sensors, including their mutual alignment.

Figure 1 provides an overview of different aspects and their mutual interrelation. The sensors play a central role and can be located in different ways (collocated, distributed, mobile) producing measurements of the same or of a different type. Fusion of heterogeneous sensor data is of particular importance, such as the combination of kinematic measurements with measured attributes providing information on the classes to which objects belongs to. In the context of defense and security applications especially, the distinction between active and passive sensing is important since passive sensors enable covert surveillance, which does not reveal itself by emitting radiation. Multifunctional sensor systems offer additional operational modes, thus requiring more intelligent strategies of sensor management that provide feedback via control or correction commands to the process of information acquisition. By this the surveillance objectives can often be reached more efficiently. Context information is given, for example, by available knowledge on the sensor and object properties, which is often quantitatively described by statistical models. Context knowledge is also environmental information on roads or topographical occlusions (GIS: Geographical Information Systems). Seen from a different perspective, context information, such as road maps, can be extracted from real-time sensor data as well [27]. Militarily relevant context knowledge (e.g. doctrines, planning data, tactics) and human observer reports (HUMINT: Human Intelligence) is also important information in the fusion process [4]. The exploitation of context information of any kind can significantly improve the fusion system performance.

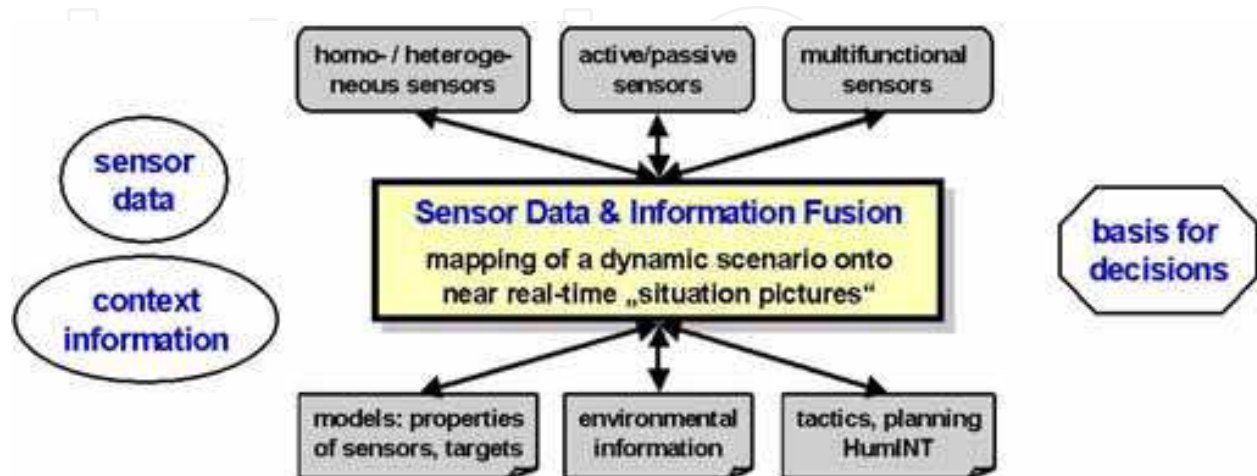


Fig. 1. Sensor data and information fusion for situation pictures: overview of characteristic aspects and their mutual interrelation.

The information elements required for producing a timely situation picture are provided by an integrative, spatio-temporal processing of the various pieces of information available, which in themselves often have only limited value for understanding the situation. Essentially, within the fusion process logical cross-references, inherent complementarity, and redundancy are exploited. More concretely speaking, the methods used are characterized by a stochastic approach (estimating relevant state quantities) and a more heuristically defined knowledgebased approach (imitating the actual human behavior when exploiting information). Besides the operational requirements, this more or less coherent methodology is the second building principle, which gives the field of sensor data and information fusion its characteristic shape.

C. Overview of a Generic Tracking System

Among the fusion products, so-called 'tracks' are of particular importance. Tracks represent knowledge on relevant state quantities of individual objects, object groups such as convoys and formations, or even large object aggregations (e.g. march columns). The information obtained by 'tracking' [6], [2], [22] includes in particular the history of the objects. If possible, a one-to-one association between the objects/object groups and the tracks is to be established and has to be preserved as long as possible (track continuity). Quantitative measures describing the quality of this knowledge are important constituents of tracks. The achievable track quality, however, does not only depend on the sensor performance, but also on the operational conditions within the actually considered scenario and the available context knowledge.

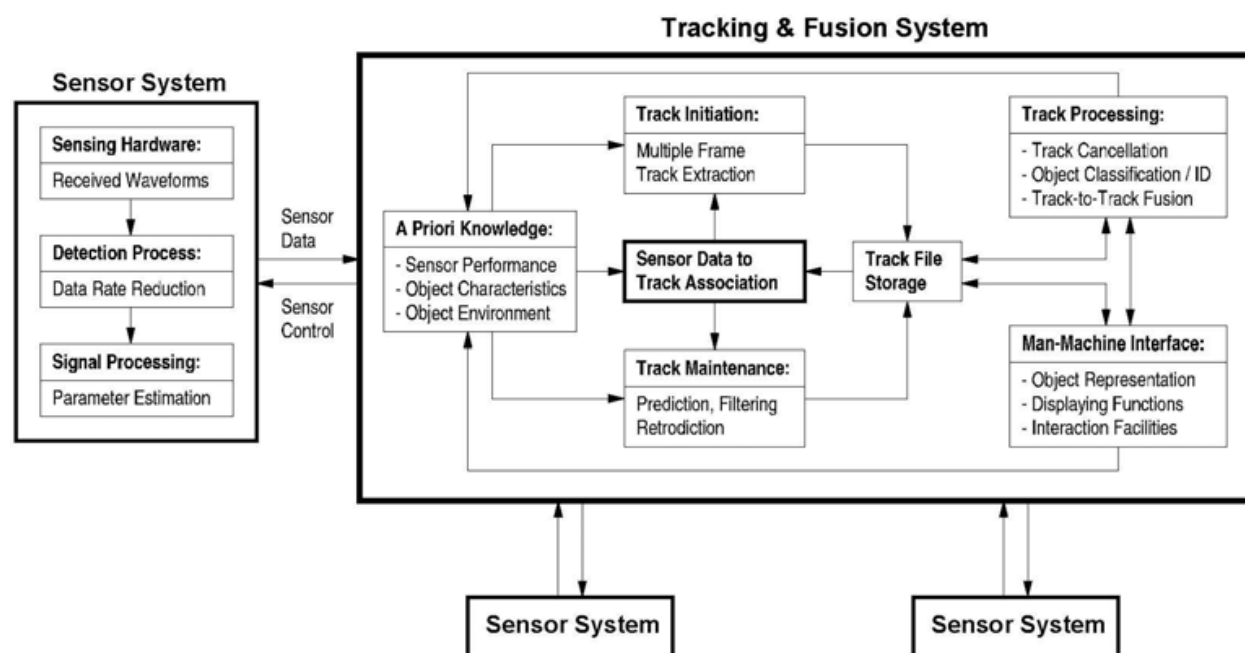


Fig. 2. Generic scheme of functional building blocks within a tracking/fusion system along with its relation to the sensors (centralized configuration, type IV according to O. Drummond).

Figure 2 shows a generic scheme of functional building blocks within a tracking/fusion system along with its relation to the underlying sensors. After passing a detection process, essentially working as a means of data rate reduction, the signal processing provides

estimates of parameters characterizing the waveforms received at the sensors' front ends (e.g. radar antennas). From these estimates sensor reports are created, i.e. measured quantities possibly related to objects of interest, which are the input for the tracking/fusion system. All sensor data that can be associated to existing tracks are used for track maintenance (using, e.g., prediction, filtering, and retrodiction). The remaining data are processed for initiating new tentative tracks (multiple frame track extraction). Association techniques thus play a key role in tracking/fusion applications. Context information in terms of statistical models (sensor performance, object characteristics, object environment) is a prerequisite to track maintenance and initiation. Track confirmation/termination, classification/identification, and fusion of tracks related to the same objects or object groups is part of the track processing. The scheme is completed by a man-machine interface with displaying and interaction functions. Context information can be updated or modified by direct human interaction or by the track processor itself, for example as a consequence of object classification or road map extraction. In the case of multifunctional sensors, feedback exists from the tracking system to the process of sensor data acquisition (sensor management).

D. A Characteristic Application: Sensor Management

Modern multifunctional agile-beam radar based on phased-array technology is an excellent example for a sensor system that requires sophisticated sensor management algorithms. This is particularly true for multiple object tracking tasks where such systems call for algorithms that efficiently exploit their degrees of freedom, which are variable over a wide range and may be chosen individually for each track. Of special interest are military air situations where both agile objects and objects significantly differing in their radar cross section must be taken into account. Unless properly handled, such situations can be highly allocation time- and energy-consuming. In this context, advanced sensor and dynamics models for combined tracking and sensor management are discussed, i.e. control of data innovation intervals, radar beam positioning, and transmitted energy management. By efficiently exploiting its limited resources, the total surveillance performance of the sensor system can be much improved.

Figure 3 shows a simplified scheme illustrating the information flow in tracking-driven phasedarray radar management. The starting point is the tracking system, which generates a request for new sensor information based on the current quality of an already established individual object track or on the requirement of initiating new tracks. We thus distinguish between track update and search requests, which enter into the priority management unit where its rank is evaluated based on the current threat or overload situation, for example, thus enabling graceful system degradation when necessary.

For each preparation of a radar system allocation, track-specific radar parameters must be set, such as the calculated radar revisit time and the corresponding radar beam position, range and Doppler-gates, or the type of the radar wave forms to be transmitted. Track search requests require the setting of appropriate revisit intervals, search sectors and patterns, and other radar parameters. In the dwell scheduling unit these preparations are transformed into antenna commands, by which the radar sensor is allocated and radar energy transmitted. The received echo signals pass a detection unit. If no detection occurs in the track maintenance mode, a local search procedure is initiated, new radar parameters are set, and a subsequent radar sensor allocation is started with as small a time delay as possible. This local search loop is repeated until either a valid detection is produced or the track is

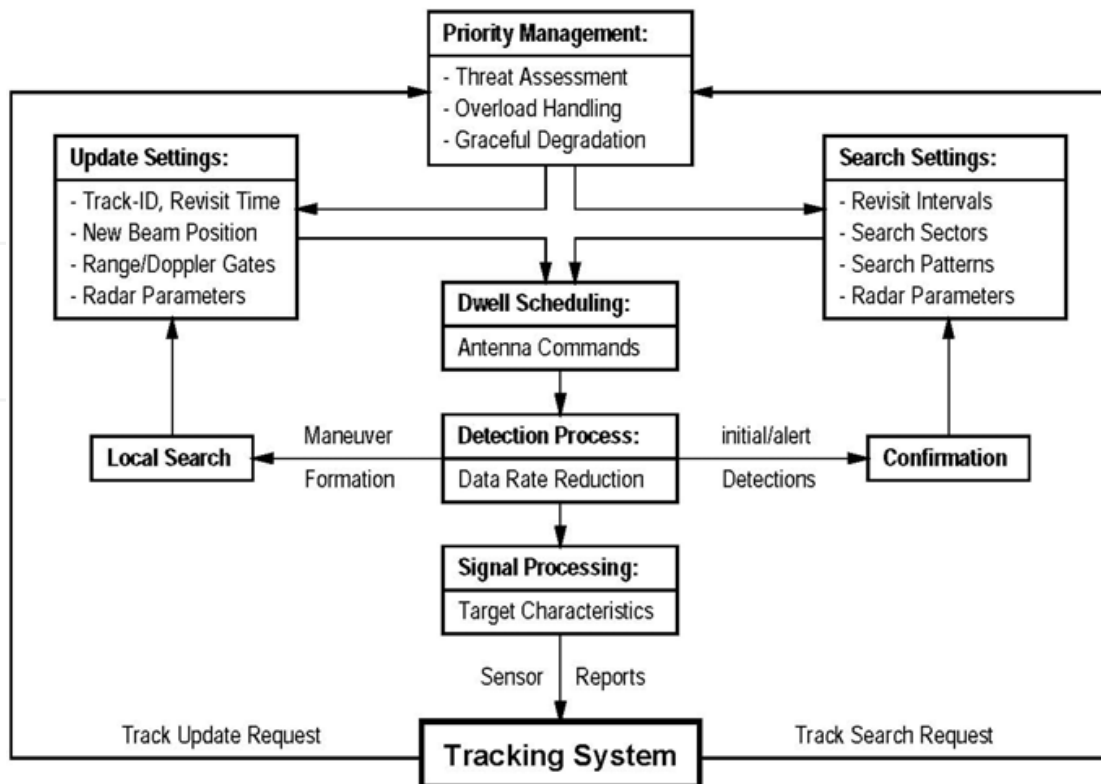


Fig. 3. Simplified scheme of the information flow in tracking-driven phased-array radar management.

canceled. While a new beam position according to a global or sector search pattern is calculated if no detection occurs in the track search mode, a tentative detection has to be confirmed before a new track is finally established. After a successful detection, the received signal passes the signal processing unit, where characteristic object parameters, such as object range, azimuth angle, radial velocity, and the object strength, are estimated being the input for the tracking system. This closes the data processing and sensor management loop. In military applications, distinct maneuvering phases often exist, since even agile objects do not maneuver permanently. Nevertheless, abrupt transitions to high- g turns can well occur. Allocation time and energy savings are thus to be expected if adaptive dynamics models of the object dynamics are used. Besides their kinematic characteristics, the mean radar cross section (RCS) of the objects to be tracked is usually unknown and variable over a wide range. By processing of signal amplitude information, however, the energy spent for track maintenance can be adapted to the actual object strength. By this measure the total sensor load can also be significantly reduced.

Due to the locally confined object illumination by the pencil-beam of a phased-array radar, abrupt transitions into maneuvering flight phases are critical since, in contrast to more conventional track-while-scan radar, a periodic object illumination is no longer guaranteed. Any track reinitiation is thus highly allocation time- and energy-consuming and also locks the sensor for other tasks (e.g. weapon guidance or providing communications links). This calls for intelligent algorithms for beam positioning and local search [17], [24], [20] that are crucial to phased-array radar tracking.

For track-while-scan radar systems, Bayesian tracking techniques are well-established. They provide an iterative updating scheme for conditional probability densities of the object state,

given all sensor data and a priori information available. In those applications data acquisition and tracking are completely decoupled. For phased-array radar, however, the current signal-to-noise ratio of the object (i.e. the detection probability) strongly depends on the correct positioning of the pencil-beam, which is now taken into the responsibility of the tracking system. Sensor control and data processing are thus closely interrelated. This basically *local* character of the tracking process constitutes the principal difference between phased-array and track-while-scan applications from a tracking point of view. By using suitable sensor models, however, this fact can be incorporated into the Bayesian formalism. The potential of this approach is thus also available for phased-array radar. The more difficult problem of global optimization, taking successive allocations into account, is not addressed here.

2. Sensor and dynamics models in bayesian object tracking

Fusing data produced at different instants of time, i.e. the tracking problem, is typically characterized by uncertainty and ambiguities, which are inherent in the underlying scenario, the object dynamics, and the sensors used. The Bayesian approach provides a well-suited methodology for dealing with many of these phenomena. More concretely speaking, the Bayesian approach provides a processing scheme for dealing with uncertain information (of a particular type), which also allows to make 'delayed' decisions if a unique decision cannot be made in a particular data situation. Ambiguities can have different causes: Sensors may produce ambiguous data due to their limited resolution capabilities or due to phenomena such as Doppler blindness in MTI radar (MTI: Moving Target Indicator). Often the objects' environment is a source of ambiguities itself (dense object situations, residual clutter, man-made noise, unwanted objects). A more indirect type of ambiguities arises from the objects' behavior (e.g. qualitatively distinct maneuvering phases). Finally, the context knowledge to be exploited can imply problem-inherent ambiguities as well, such as intersections in road maps or ambiguous tactical rules describing the over-all object behavior. The general multiple-object, multiple-sensor tracking task, however, is highly complex and involves sophisticated combinatorial considerations that are beyond the scope of this chapter (see [5], [30] as an introduction). Nevertheless, in many applications, the tracking task can be partitioned into independent sub-problems of (much) less complexity.

According to this discussion, we proceed along the following lines.

- *Basis:* In the course of time, one or several sensors produce measurements of one or more objects of interest. The accumulated sensor data are an example of a 'time series'. Each object is characterized by its current 'state', a vector typically consisting of the current object position, its velocity, and acceleration.
- *Objective:* Learn as much as possible about the individual object states at each time of interest by analyzing the 'time series' created by the sensor data.
- *Problem:* The sensor information is inaccurate, incomplete, and possibly even ambiguous. Moreover, the objects' temporal evolution is usually not well-known.
- *Approach:* Interpret sensor measurements and object state vectors as random variables. Describe by probability density functions (pdfs) what is known about these random variables.
- *Solution:* Derive iteration formulae for calculating the probability density functions of the state variables and develop a mechanism for initiating the iteration. Derive state estimates from the pdfs along with appropriate quality measures.

A. The Key-role of Bayes' Formula

At particular instants of time denoted by $t_l, l = 1, \dots, k$, we consider the set $Z_l = \{z_l^1, \dots, z_l^{n_l}\}$ of n_l measurements related to the object state \mathbf{x}_l . In case of multiple objects \mathbf{x}_l is the joint state. The corresponding time series up to and including t_k is recursively defined by $\mathcal{Z}^k = \{Z_k, n_k, \mathcal{Z}^{k-1}\}$. The central question of object tracking is: What can be known about the object states \mathbf{x}_l at time instants t_l , i.e. for the past ($l < k$), at present ($l = k$), and in the future ($l > k$), by exploiting the sensor data collected in the times series \mathcal{Z}^k ? According to the approach previously sketched, the answer is given by the conditional probability density functions (pdf) $p(\mathbf{x}_l | \mathcal{Z}^k)$ to be calculated iteratively as a consequence of Bayes' rule. For $l = k$, i.e. for object states at the current time t_k , we obtain:

$$p(\mathbf{x}_k | \mathcal{Z}^k) = \frac{p(Z_k, n_k | \mathbf{x}_k) p(\mathbf{x}_k | \mathcal{Z}^{k-1})}{\int d\mathbf{x}_k p(Z_k, n_k | \mathbf{x}_k) p(\mathbf{x}_k | \mathcal{Z}^{k-1})}. \quad (1)$$

In other words, $p(\mathbf{x}_k | \mathcal{Z}^k)$ can be calculated from the pdfs $p(\mathbf{x}_k | \mathcal{Z}^{k-1})$ and $p(Z_k, n_k | \mathbf{x}_k)$. $p(\mathbf{x}_k | \mathcal{Z}^{k-1})$ describes, what is known on \mathbf{x}_k given all past sensor data \mathcal{Z}^{k-1} , i.e. a prediction. Obviously, $p(Z_k, n_k | \mathbf{x}_k)$ needs to be known up to a constant factor only. Any function

$$\ell(\mathbf{x}_k; Z_k, n_k) \propto p(Z_k, n_k | \mathbf{x}_k) \quad (2)$$

produces the same result. Functions of this type are also called *likelihood functions* and describe what can be learned from the current sensor output Z_k, n_k about the object state \mathbf{x}_k at this time. This is the reason, why likelihood functions are often also called "sensor models", since they mathematically represent the sensor, its measurements and properties, in the data processing formalism. For well-separated objects, perfect detection, in absence of false returns, and for bias-free measurements of linear functions $\mathbf{H}_k \mathbf{x}_k$ of the object state with a Gaussian, white noise measurement error characterized by a covariance matrix \mathbf{R}_k , the likelihood functions are proportional to a Gaussian: $\ell(\mathbf{x}_k; \mathbf{z}_k, \mathbf{H}_k, \mathbf{R}_k) \propto \mathcal{N}(\mathbf{z}_k; \mathbf{H}_k \mathbf{x}_k, \mathbf{R}_k)$.

B. Prediction Update Step

The pdf $p(\mathbf{x}_k | \mathcal{Z}^{k-1})$ in the Equation 1 is a prediction of the knowledge on the object state for the time t_k based on all the measurements received up to and including time t_{k-1} . By writing this pdf as a marginal density, $p(\mathbf{x}_k | \mathcal{Z}^{k-1}) = \int d\mathbf{x}_{k-1} p(\mathbf{x}_k, \mathbf{x}_{k-1} | \mathcal{Z}^{k-1})$, the object state \mathbf{x}_{k-1} at the previous time t_{k-1} comes into play yielding:

$$p(\mathbf{x}_k | \mathcal{Z}^{k-1}) = \int d\mathbf{x}_{k-1} \underbrace{p(\mathbf{x}_k | \mathbf{x}_{k-1}, \mathcal{Z}^{k-1})}_{\text{object dynamics}} \underbrace{p(\mathbf{x}_{k-1} | \mathcal{Z}^{k-1})}_{\text{previous posterior}}. \quad (3)$$

The state transition density $p(\mathbf{x}_k | \mathbf{x}_{k-1}, \mathcal{Z}^{k-1})$ is often called the "object dynamics model" and mathematically represents the kinematic object properties in the data processing formalism in the same way as the likelihood function represents the sensor(s).

1) *Gauss-Markov Dynamics*: A Gauss-Markov dynamics, defined by the transition density

$$p(\mathbf{x}_k | \mathbf{x}_{k-1}, \mathcal{Z}^{k-1}) = \mathcal{N}(\mathbf{x}_k; \mathbf{F}_{k|k-1} \mathbf{x}_{k-1}, \mathbf{D}_{k|k-1}), \quad (4)$$

is characterized by the modeling parameters $\mathbf{F}_{k|k-1}$ (evolution matrix), describing the deterministic part of the temporal evolution, and $\mathbf{D}_{k|k-1}$ (dynamics covariance matrix), characterizing its stochastic part. If we additionally assume that the previous posterior is a Gaussian, given by

$$p(\mathbf{x}_{k-1} | \mathcal{Z}^{k-1}) = \mathcal{N}(\mathbf{x}_{k-1}; \mathbf{x}_{k-1|k-1}, \mathbf{P}_{k-1|k-1}), \quad (5)$$

$p(\mathbf{x}_k | \mathcal{Z}^{k-1})$ is also a Gaussian:

$$p(\mathbf{x}_k | \mathcal{Z}^{k-1}) = \mathcal{N}(\mathbf{x}_k; \mathbf{x}_{k|k-1}, \mathbf{P}_{k|k-1}) \quad (6)$$

with an expectation vector $\mathbf{x}_{k|k-1}$ and a covariance matrix $\mathbf{P}_{k|k-1}$ given by:

$$\mathbf{x}_{k|k-1} = \mathbf{F}_{k|k-1} \mathbf{x}_{k-1|k-1} \quad (7)$$

$$\mathbf{P}_{k|k-1} = \mathbf{F}_{k|k-1} \mathbf{P}_{k-1|k-1} \mathbf{F}_{k|k-1}^\top + \mathbf{D}_{k|k-1}. \quad (8)$$

This directly results from a useful product formula for Gaussians¹:

$$\mathcal{N}(\mathbf{z}; \mathbf{H}\mathbf{x}, \mathbf{R}) \mathcal{N}(\mathbf{x}; \mathbf{y}, \mathbf{P}) = \mathcal{N}(\mathbf{z}; \mathbf{H}\mathbf{y}, \mathbf{S}) \times \begin{cases} \mathcal{N}(\mathbf{x}; \mathbf{y} + \mathbf{W}\boldsymbol{\nu}, \mathbf{P} - \mathbf{W}\mathbf{S}\mathbf{W}^\top) \\ \mathcal{N}(\mathbf{x}; \mathbf{Q}(\mathbf{P}^{-1}\mathbf{x} + \mathbf{H}^\top \mathbf{R}^{-1}\mathbf{z}), \mathbf{Q}) \end{cases}, \quad (9)$$

where we used the abbreviations:

$$\boldsymbol{\nu} = \mathbf{z} - \mathbf{H}\mathbf{y}, \quad \mathbf{S} = \mathbf{H}\mathbf{P}\mathbf{H}^\top + \mathbf{R}, \quad \mathbf{W} = \mathbf{P}\mathbf{H}^\top \mathbf{S}^{-1}, \quad \mathbf{Q}^{-1} = \mathbf{P}^{-1} + \mathbf{H}^\top \mathbf{R}^{-1}\mathbf{H}. \quad (10)$$

Note that after applying this formula the integration variable \mathbf{x}_{k-1} in the Equation 3 is no longer contained in the first Gaussian of the product. The integration becomes thus trivial as pdfs are normalized.

2) *IMM Dynamics Model*: In practical applications, it might be uncertain which dynamics model out of a set of possible alternatives is currently in effect. Such cases, e.g. objects characterized by different modes of dynamical behavior, can be handled by multiple dynamics models with a given probability of switching between them (IMM: Interacting Multiple Models, [2], [6] and the literature cited therein). The model transition probabilities are thus part of the modeling assumptions. More strictly speaking, suppose that r models are given and let j_k be denoting the dynamics model assumed to be in effect at time t_k , the statistical properties of systems with Markovian switching coefficients are summarized by the following equation:

$$p(x_k, j_k | x_{k-1}, j_{k-1}) = p(x_k | x_{k-1}, j_k) p(j_k | j_{k-1}) \quad (11)$$

¹Sketch of proof: Interpret $\mathcal{N}(\mathbf{z}; \mathbf{H}\mathbf{x}, \mathbf{R})\mathcal{N}(\mathbf{x}; \mathbf{y}, \mathbf{P})$ as a joint density $p(\mathbf{z}, \mathbf{x}) = p(\mathbf{z} | \mathbf{x})p(\mathbf{x})$. It can be written as a Gaussian, from which the marginal and conditional densities $p(\mathbf{z})$, $p(\mathbf{x} | \mathbf{z})$ can be derived. In the calculations make use of known formulae for the inverse of a partitioned matrix (see [2, p. 22], e.g.). From $p(\mathbf{z}, \mathbf{x}) = p(\mathbf{x} | \mathbf{z})p(\mathbf{z})$ the formula results.

$$= p(j_k | j_{k-1}) \mathcal{N}(\mathbf{x}_k; \mathbf{F}_{k|k-1}^{j_k} \mathbf{x}_{k-1}, \mathbf{D}_{k|k-1}^{j_k}). \quad (12)$$

For $r = 1$, the previous linear-Gaussian model results as a limiting case. Fortunately, the tracking performance does not seem to critically depend on the particular choice of the model transition probabilities $p(j_k | j_{k-1})$, provided the number r of models involved is small [7].

Let us assume that the previous posterior is written as a Gaussian mixture,

$$p(\mathbf{x}_{k-1} | \mathcal{Z}^{k-1}) = \sum_{j_{k-1}=1}^r \cdots \sum_{j_{k-n}=1}^r p(\mathbf{x}_{k-1}, j_{k-1}, \dots, j_{k-n} | \mathcal{Z}^{k-1}) \quad (13)$$

$$= \sum_{\mathbf{j}_{k-1}} p(\mathbf{x}_{k-1}, \mathbf{j}_{k-1} | \mathcal{Z}^{k-1}) \quad (14)$$

$$= \sum_{\mathbf{j}_{k-1}} p(\mathbf{j}_{k-1} | \mathcal{Z}^{k-1}) \mathcal{N}(\mathbf{x}_{k-1}; \mathbf{x}_{k-1|k-1}^{\mathbf{j}_{k-1}}, \mathbf{P}_{k-1|k-1}^{\mathbf{j}_{k-1}}), \quad (15)$$

i.e. a weighted sum of individual Gaussians. The vector index \mathbf{j}_{k-1} is defined by $\mathbf{j}_{k-1} = j_{k-1}, j_{k-2}, \dots, j_{k-n}$, i.e. the mixture $p(\mathbf{x}_{k-1} | \mathcal{Z}^{k-1})$ is given by r^n components, where n is a parameter. The case $n = 1$ corresponds to the situation standard IMM prediction [2, p. ???ff]. With a previous posterior of this type, we obtain for the prediction update:

$$p(\mathbf{x}_k | \mathcal{Z}^{k-1}) = \sum_{j_k=1}^r \sum_{\mathbf{j}_{k-1}} \int d\mathbf{x}_{k-1} p(\mathbf{x}_k, j_k | \mathbf{x}_{k-1}, j_{k-1}) p(\mathbf{x}_{k-1}, \mathbf{j}_{k-1} | \mathcal{Z}^{k-1}) \quad (16)$$

$$= \sum_{j_k=1}^r \sum_{\mathbf{j}_{k-1}} p_{k|k-1}^{j_k, \mathbf{j}_{k-1}} \mathcal{N}(\mathbf{x}_k; \mathbf{x}_{k|k-1}^{j_k, \mathbf{j}_{k-1}}, \mathbf{P}_{k|k-1}^{j_k, \mathbf{j}_{k-1}}) \quad (17)$$

$$= \sum_{\mathbf{j}_k} \sum_{j_{k-1}=1}^r p_{k|k-1}^{\mathbf{j}_k, j_{k-1}} \mathcal{N}(\mathbf{x}_k; \mathbf{x}_{k|k-1}^{\mathbf{j}_k, j_{k-1}}, \mathbf{P}_{k|k-1}^{\mathbf{j}_k, j_{k-1}}) \quad (18)$$

with weighting factors $p_{k|k-1}^{j_k, \mathbf{j}_{k-1}}$, an expectation vector $\mathbf{x}_{k|k-1}^{j_k, \mathbf{j}_{k-1}}$, and a covariance matrix $\mathbf{P}_{k|k-1}^{j_k, \mathbf{j}_{k-1}}$ given by:

$$p_{k|k-1}^{j_k, \mathbf{j}_{k-1}} = p(j_k | \mathbf{j}_{k-1}) p(\mathbf{j}_{k-1} | \mathcal{Z}^{k-1}) \quad (19)$$

$$\mathbf{x}_{k|k-1}^{j_k, \mathbf{j}_{k-1}} = \mathbf{F}_{k|k-1}^{j_k} \mathbf{x}_{k-1|k-1}^{\mathbf{j}_{k-1}} \quad (20)$$

$$\mathbf{P}_{k|k-1}^{j_k, \mathbf{j}_{k-1}} = \mathbf{F}_{k|k-1}^{j_k} \mathbf{x}_{k-1|k-1}^{\mathbf{j}_{k-1}} \mathbf{F}_{k|k-1}^{j_k \top} + \mathbf{D}_{k|k-1}^{j_k} \quad (21)$$

by exploiting the product formula (Equation 9). From these considerations follows that the number of mixture components is continuously increasing in each prediction update step.

Via moment matching [2, p. 56], the number of mixture components can be kept constant if the sum over j_{k-n} in Equation 18 is approximated by:

$$\sum_{j_{k-n}=1}^r p_{k|k-1}^{\mathbf{j}_{k,j_{k-1}}} \mathcal{N}(\mathbf{x}_k; \mathbf{x}_{k|k-1}^{\mathbf{j}_{k,j_{k-1}}}, \mathbf{P}_{k|k-1}^{\mathbf{j}_{k,j_{k-1}}}) \approx p(\mathbf{j}_k | \mathcal{Z}^{k-1}) \mathcal{N}(\mathbf{x}_k; \mathbf{x}_{k|k-1}^{\mathbf{j}_k}, \mathbf{P}_{k|k-1}^{\mathbf{j}_k}), \quad (22)$$

with $p(\mathbf{j}_k | \mathcal{Z}^{k-1})$, $\mathbf{x}_{k|k-1}^{\mathbf{j}_k}$, and $\mathbf{P}_{k|k-1}^{\mathbf{j}_k}$ given by:

$$p_{k|k-1}^{\mathbf{j}_k} = \sum_{j_{k-n}=1}^r p_{k|k-1}^{\mathbf{j}_{k,j_{k-1}}} \quad (23)$$

$$\mathbf{x}_{k|k-1}^{\mathbf{j}_k} = \frac{1}{p_{k|k-1}^{\mathbf{j}_k}} \sum_{j_{k-n}=1}^r p_{k|k-1}^{\mathbf{j}_{k,j_{k-1}}} \mathbf{x}_{k|k-1}^{\mathbf{j}_{k,j_{k-1}}} \quad (24)$$

$$\mathbf{P}_{k|k-1}^{\mathbf{j}_k} = \frac{1}{p_{k|k-1}^{\mathbf{j}_k}} \sum_{j_{k-n}=1}^r p_{k|k-1}^{\mathbf{j}_{k,j_{k-1}}} (\mathbf{P}_{k|k-1}^{\mathbf{j}_{k,j_{k-1}}} + (\mathbf{x}_{k|k-1}^{\mathbf{j}_{k,j_{k-1}}} - \mathbf{x}_{k|k-1}^{\mathbf{j}_k})(\mathbf{x}_{k|k-1}^{\mathbf{j}_{k,j_{k-1}}} - \mathbf{x}_{k|k-1}^{\mathbf{j}_k})^\top) \quad (25)$$

yielding a Gaussian sum representation of $p(\mathbf{x}_k | \mathcal{Z}^{k-1})$ with r^m mixture components.

C. Filtering Update Step

According to previous considerations, the conditional pdf $p(\mathbf{x}_k | \mathcal{Z}^k)$ can be calculated iteratively by combining the following pieces of evidence: $p(\mathbf{x}_{k-1} | \mathcal{Z}^{k-1})$ (knowledge of the past), $p(\mathbf{x}_k | \mathbf{x}_{k-1})$ (object dynamics), $\ell(\mathbf{x}_k; \mathcal{Z}_k, n_k)$ (measurements, sensor model).

1) *Standard Kalman Update Formulae*: In case of well-separated objects under ideal conditions, i.e. without false returns, assuming perfect detection, a single dynamics model, and Gaussian measurement errors, the well-known Kalman filtering results as a limiting case of this more general Bayesian approach. The Kalman filter is thus a simple straight-forward realization of Bayesian tracking. In this idealized situation, i.e. with:

$$p(\mathbf{x}_k | \mathbf{x}_{k-1}) = \mathcal{N}(\mathbf{x}_k; \mathbf{F}_{k|k-1} \mathbf{x}_{k-1}, \mathbf{D}_{k|k-1}) \quad (26)$$

$$\ell(\mathbf{x}_k; \mathbf{z}_k) = \mathcal{N}(\mathbf{z}_k; \mathbf{H}_k \mathbf{x}_k, \mathbf{R}_k), \quad (27)$$

Equation 1 provides Gaussian pdfs,

$$p(\mathbf{x}_k | \mathcal{Z}^k) = \mathcal{N}(\mathbf{x}_k; \mathbf{x}_{k|k}, \mathbf{P}_{k|k}), \quad (28)$$

representing the available knowledge at each time t_k . According to the previous product formula (Equation 9), we obtain two equivalent versions of the Kalman update equations for $\mathbf{x}_{k|k}$, $\mathbf{P}_{k|k}$:

$$\mathbf{x}_{k|k} = \begin{cases} \mathbf{x}_{k|k-1} + \mathbf{W}_{k|k-1} (\mathbf{z}_k - \mathbf{H}_k \mathbf{x}_{k|k-1}) \\ \mathbf{P}_{k|k} (\mathbf{P}_{k|k-1}^{-1} \mathbf{x}_{k|k-1} + \mathbf{H}_k^\top \mathbf{R}_k^{-1} \mathbf{z}_k) \end{cases} \quad (29)$$

$$\mathbf{P}_{k|k} = \begin{cases} \mathbf{P}_{k|k-1} - \mathbf{W}_{k|k-1} \mathbf{S}_{k|k-1} \mathbf{W}_{k|k-1}^\top \\ (\mathbf{P}_{k|k-1}^{-1} + \mathbf{H}_k^\top \mathbf{R}_k^{-1} \mathbf{H}_k)^{-1} \end{cases} \quad (30)$$

with the Kalman Gain Matrix $\mathbf{W}_{k|k-1}$ and the Innovation Covariance Matrix $\mathbf{S}_{k|k-1}$, given by

$$\mathbf{W}_{k|k-1} = \mathbf{P}_{k|k-1} \mathbf{H}_{k|k-1}^\top \mathbf{S}_{k|k-1}^{-1}, \quad (31)$$

$$\mathbf{S}_{k|k-1} = \mathbf{H}_k \mathbf{P}_{k|k-1} \mathbf{H}_k^\top + \mathbf{R}_k. \quad (32)$$

At time t_0 , the pdf $p(\mathbf{x}_0 | \mathcal{Z}^0) = \mathcal{N}(\mathbf{x}_0; \mathbf{x}_0|_0, \mathbf{P}_0|_0)$ describes the initial knowledge on the object kinematics. As an example, let us consider state vectors $\mathbf{x}_k = (\mathbf{r}_k^\top, \dot{\mathbf{r}}_k^\top)^\top$, consisting of the object position and velocity, and position measurements \mathbf{z}_k with measurement error covariance matrices \mathbf{R}_k . Based on a first measurement \mathbf{z}_0 and the context information that v_{\max} is a measure of the maximum object speed to be expected, a reasonable initiation is given by $\mathbf{x}_0|_0 = (\mathbf{z}_0^\top, \mathbf{0}^\top)^\top$, $\mathbf{P}_0|_0 = \text{diag}[\mathbf{R}_0, v_{\max}^2 \mathbf{1}]$.

2) *More Sophisticated Sensor Models:* A very simple example illustrates, in which way negative sensor evidence, i.e. an expected but actually missing sensor measurement, is to be treated within the Bayesian formalism. Let us first exclude false measurements and assume that the objects of interest are detected with a constant detection probability $P_D < 1$. This problem is thus identical with the previously discussed Kalman filtering except that measurements are not at each time t_k available. In this case, the underlying sensor model, i.e. the likelihood function, has not only to describe the measurement process, characterized by the measurement matrix \mathbf{H}_k and the measurement error covariance matrix \mathbf{R}_k , but also the detection process, characterized by the detection probability $P_D < 1$. According to this discussion, there exist two possibilities: either the object was detected at time t_k (data interpretation hypothesis $i_k = 1$, or not (data interpretation hypothesis $i_k = 0$). Under the assumption that the probabilities $p(i_k = 1 | \mathbf{x}_k) = P_D$ and $P(i_k = 0 | \mathbf{x}_k) = 1 - P_D$ do not depend on the object state \mathbf{x}_k , we obtain with $\delta_{ij} = 0$ for $i \neq j$ and $\delta_{ij} = 1$ for $i = j$ the following likelihood function:

$$p(Z_k, n_k | \mathbf{x}_k) = \sum_{i_k=0}^1 p(Z_k, n_k, i_k | \mathbf{x}_k) = \sum_{i_k=0}^1 p(Z_k, n_k | i_k, \mathbf{x}_k) p(i_k | \mathbf{x}_k) \quad (33)$$

$$= \delta_{0, n_k} (1 - P_D) + \delta_{1, n_k} P_D \mathcal{N}(\mathbf{z}_k; \mathbf{H} \mathbf{x}_k, \mathbf{R}) \quad (34)$$

$$=: \ell(\mathbf{x}_k; \mathbf{z}_k, \mathbf{H}_k, \mathbf{R}_k, P_D). \quad (35)$$

With $p(\mathbf{x}_k | \mathcal{Z}^{k-1}) = \mathcal{N}(\mathbf{x}_k; \mathbf{x}_k|_{k-1}, \mathbf{P}_k|_{k-1})$, Equation 1 leads to the following conclusions:

1. For a positive sensor output ($n_k = 1$) the measurement \mathbf{z}_k is processed via Kalman filtering resulting in $p(\mathbf{x}_k | \mathcal{Z}^k) = \mathcal{N}(\mathbf{x}_k; \mathbf{x}_k|_k, \mathbf{P}_k|_k)$ with $\mathbf{x}_k|_k$ and $\mathbf{P}_k|_k$ given by Equations 29 and 30.
2. For a negative sensor output ($n_k = 0$) the likelihood function is given by the constant $1 - P_D$. This implies that prediction pdf is not modified in the filtering step: $\mathbf{x}_k|_k = \mathbf{x}_k|_{k-1}$.

$\mathbf{P}_{k|k} = \mathbf{P}_{k|k-1}$. According to the Kalman update equations this result can formally be interpreted as a processing of a *pseudo*-measurement with an infinitely large measurement error covariance matrix \mathbf{R}'_k , since in this case $\mathbf{R}'_k{}^{-1}=0$.

The Bayesian formalism and the sensor model (likelihood function) obviously define how a negative sensor output, i.e. a missing detection is to be processed.

In the case of well-separated objects in the presence of false returns and imperfect detection, the n_k sensor data Z_k are also not longer uniquely interpretable. Let $i_k = 0$ denote the data interpretation hypothesis that the object has not been detected at time t_k , all sensor data being false returns, while $i_k = i, i = 1, \dots, n_k$ represents the hypothesis that the object has been detected, $\mathbf{z}_k^i \in Z_k$ being a object measurement, the remaining sensor data being false returns. Evidently, $\{i_k^i\}_{i=0}^{n_k}$ is a set of mutually exclusive and exhaustive data interpretations. Due to the total probability theorem, the corresponding likelihood function is thus given by:

$$\ell(\mathbf{x}_k; Z_k, n_k) = \sum_{i_k=0}^{n_k} p(Z_k, n_k | i_k, \mathbf{x}_k) p(i_k | \mathbf{x}_k) \quad (36)$$

$$= \sum_{i_k=0}^{n_k} p(Z_k | n_k, i_k, \mathbf{x}_k) p(n_k | i_k, \mathbf{x}_k) p(i_k | \mathbf{x}_k) \quad (37)$$

$$= |\text{FoV}|^{-n_k} p_F(n_k)(1 - P_D) + |\text{FoV}|^{-(n_k-1)} p_F(n_k - 1) \left[\frac{1}{n_k} P_D \right] \sum_{i_k=1}^{n_k} \mathcal{N}(\mathbf{z}_k^{i_k}; \mathbf{H}_k^{i_k} \mathbf{x}_k, \mathbf{R}_k^{i_k}) \quad (38)$$

$$\propto (1 - P_D) \rho_F + P_D \sum_{i_k=1}^{n_k} \mathcal{N}(\mathbf{z}_k^{i_k}; \mathbf{H}_k^{i_k} \mathbf{x}_k, \mathbf{R}_k^{i_k}), \quad (39)$$

where we assumed a constant detection probability P_D and false returns equally distributed in the field of view $|\text{FoV}|$ and Poisson distributed in number; i.e. the probability of having n false returns is given by $p_F(n) = \frac{\rho_F |\text{FoV}|^n}{n!} e^{-\rho_F |\text{FoV}|}$ with a spatial false return density ρ_F and $|\text{FoV}|$ denoting the volume of the field of view. See [22] for a more detailed discussion. According to the Equation 1, this likelihood function implies that $p(\mathbf{x}_k | Z^k)$ becomes a Gaussian mixture, a weighted sum of Gaussians, whose parameters are obtained by exploiting the product formula (9).

D. Gaussian Mixtures and Multiple Hypothesis Tracking

In many applications, such as group target tracking with possibly unresolved measurements [26], in ground moving target tracking with STAP radar [21], or target tracking with a phasedarray radar in the presence of jamming [10], the sensor model is described by a likelihood function of the type $\ell(\mathbf{x}_k; Z_k, n_k) \propto \sum_{i_k=0}^{n_k} p(Z_k, n_k | i_k, \mathbf{x}_k) p(i_k | \mathbf{x}_k)$ [20]. Such likelihood functions, which are essentially characterized by taking different data interpretation hypotheses i_k into account, are the basis for Multiple Hypothesis Tracking algorithms (MHT, see [5]). In this context, each mixture component of the pdfs that result from Bayes' Rule and a Gaussian mixture prediction,

$$p(\mathbf{x}_k | \mathcal{Z}^k) = \sum_{\mathbf{i}_k} p_{k|k}^{\mathbf{i}_k} \mathcal{N}(\mathbf{x}_k; \mathbf{x}_{k|k}^{\mathbf{i}_k}, \mathbf{P}_{k|k}^{\mathbf{i}_k}), \quad (40)$$

represents a track hypothesis, which is characterized by a sequence of data interpretation hypotheses $\mathbf{i}_k = (i_k, i_{k-1}, \dots)$, i.e. data interpretation history.

The structure of a Gaussian mixture for $p(\mathbf{x}_k | \mathcal{Z}^k)$ also occurs if an IMM prediction $p(\mathbf{x}_k | \mathcal{Z}^{k-1})$ (see previous subsection) is updated by using a Gaussian likelihood function $\ell(\mathbf{x}_k; \mathbf{z}_k, \mathbf{H}_k, \mathbf{R}_k) = \mathcal{N}(\mathbf{z}_k; \mathbf{H}_k \mathbf{x}_k, \mathbf{R}_k)$ according to Equation 1 and the product formula (Equation 9):

$$p(\mathbf{x}_k | \mathcal{Z}^k) = \frac{\sum_{\mathbf{j}_k} p_{k|k-1}^{\mathbf{j}_k} \mathcal{N}(\mathbf{z}_k; \mathbf{H}_k \mathbf{x}_k, \mathbf{R}_k) \mathcal{N}(\mathbf{x}_k; \mathbf{x}_{k|k-1}^{\mathbf{j}_k}, \mathbf{P}_{k|k-1}^{\mathbf{j}_k})}{\sum_{\mathbf{j}_k} p_{k|k-1}^{\mathbf{j}_k} \int d\mathbf{x}_k \mathcal{N}(\mathbf{z}_k; \mathbf{H}_k \mathbf{x}_k, \mathbf{R}_k) \mathcal{N}(\mathbf{x}_k; \mathbf{x}_{k|k-1}^{\mathbf{j}_k}, \mathbf{P}_{k|k-1}^{\mathbf{j}_k})} \quad (41)$$

$$= \sum_{\mathbf{j}_k} p_{k|k}^{\mathbf{j}_k} \mathcal{N}(\mathbf{x}_k; \mathbf{x}_{k|k}^{\mathbf{j}_k}, \mathbf{P}_{k|k}^{\mathbf{j}_k}), \quad (42)$$

where the mixture parameters $p_{k|k}^{\mathbf{j}_k}$, $\mathbf{x}_{k|k}^{\mathbf{j}_k}$, and $\mathbf{P}_{k|k}^{\mathbf{j}_k}$ are given by:

$$p_{k|k}^{\mathbf{j}_k} = \frac{p_{k|k-1}^{\mathbf{j}_k} \mathcal{N}(\mathbf{z}_k; \mathbf{H}_k \mathbf{x}_{k|k-1}^{\mathbf{j}_k}, \mathbf{S}_{k|k-1}^{\mathbf{j}_k})}{\sum_{\mathbf{j}_k} p_{k|k-1}^{\mathbf{j}_k} \mathcal{N}(\mathbf{z}_k; \mathbf{H}_k \mathbf{x}_{k|k-1}^{\mathbf{j}_k}, \mathbf{S}_{k|k-1}^{\mathbf{j}_k})} \quad (43)$$

$$\mathbf{x}_{k|k}^{\mathbf{j}_k} = \mathbf{x}_{k|k-1}^{\mathbf{j}_k} + \mathbf{W}_{k|k-1}^{\mathbf{j}_k} (\mathbf{z}_k - \mathbf{H}_k \mathbf{x}_{k|k-1}^{\mathbf{j}_k}) \quad (44)$$

$$\mathbf{P}_{k|k}^{\mathbf{j}_k} = \mathbf{P}_{k|k-1}^{\mathbf{j}_k} - \mathbf{W}_{k|k-1}^{\mathbf{j}_k} \mathbf{S}_{k|k-1}^{\mathbf{j}_k} \mathbf{W}_{k|k-1}^{\mathbf{j}_k \top} \quad (45)$$

with the standard Kalman Gain and Innovation Covariance matrices

$$\mathbf{W}_{k|k-1}^{\mathbf{j}_k} = \mathbf{P}_{k|k-1}^{\mathbf{j}_k} \mathbf{H}_k^\top \mathbf{S}_{k|k-1}^{\mathbf{j}_k -1} \quad (46)$$

$$\mathbf{S}_{k|k-1}^{\mathbf{j}_k} = \mathbf{H}_k^\top \mathbf{P}_{k|k-1}^{\mathbf{j}_k} \mathbf{H}_k + \mathbf{R}_k \quad (47)$$

IMM filtering may thus be considered as a multiple 'model hypotheses' tracking method. Also combined IMM-MHT-approaches are discussed in the literature, e.g. [23]. See [34], [35] for an alternative treatment of the multiple hypothesis, multiple model tracking problem.

E. Summary and Realization Aspects

A Bayesian tracking algorithm is an iterative updating scheme for conditional probability density functions $p(\mathbf{x}_k | \mathcal{Z}^k)$ representing all available knowledge on the kinematical state vectors \mathbf{x}_k of the objects to be tracked at discrete instants of time t_k . The pdfs are conditioned by both the sensor data \mathcal{Z}^k accumulated up to some time t_k , typically the current scan time, and by available context information, such as sensor characteristics, object dynamics, environments, topographical maps, tactical rules. Depending on the time t_l at which estimates for the state vectors \mathbf{x}_l are required, the related estimation process is referred to as prediction ($t_l > t_k$) and filtering ($t_l = t_k$). In the following the iterative calculation is illustrated schematically:

$$\begin{array}{l}
 \text{prediction:} \quad p(\mathbf{x}_{k-1} | \mathcal{Z}^{k-1}) \xrightarrow[\text{kinematic constraints}]{\text{dynamics model}} p(\mathbf{x}_k | \mathcal{Z}^{k-1}) \\
 \text{filtering:} \quad p(\mathbf{x}_k | \mathcal{Z}^{k-1}) \xrightarrow[\text{sensor model}]{\text{current sensor data}} p(\mathbf{x}_k | \mathcal{Z}^k)
 \end{array} \tag{48}$$

Under more realistic conditions, the pdfs have the structure of finite mixtures, i.e. weighted sums of individual densities that assume particular data interpretations or model hypotheses to be true. This structure is a direct consequence of the uncertain origin of the sensor data and/or of the uncertainty related to the underlying system dynamics. Provided the densities $p(\mathbf{x}_k | \mathcal{Z}^k)$ are calculated correctly, optimal estimators can be derived related to various risk functions adapted to the applications. See [19] for a generalization of this Bayesian scheme to extended objects and object clusters and to retrodiction [23].

Due to the uncertain origin of the sensor data, naively applied Bayesian tracking leads to memory explosion. The number of components in the mixture densities $p(\mathbf{x}_k | \mathcal{Z}^k)$ exponentially grow at each step. Suboptimal approximation techniques are therefore inevitable in any practical realization. Fortunately, in many applications, the densities resulting from prediction and filtering are characterized by a finite number of modes that may be fluctuating and even large for a while, but does not explosively grow. This is the rationale for adaptive approximation methods that keep the number of mixture components under control without disturbing the density iteration too seriously [12], [32]. In other words, the densities can often be approximated by mixtures with (far) less components (e.g. by merging of similar and pruning of irrelevant mixture components). Provided the relevant features of the densities are preserved, the resulting suboptimal algorithms are expected to be close to optimal Bayesian filtering. For dealing with non-linearities ‘extended’ or ‘unscented’ Kalman filtering (EKF [2], UKF [14]) or particle filtering (PF [31]) can be used.

3. Example: tracking-driven phased-array radar management

Resource management for a multi-functional radar certainly depends on the particular application considered. We here discuss track maintenance for ground-based air surveillance while minimizing the allocation time and energy required. The track accuracy is important only insofar as stable tracks are guaranteed. Track initiation or implementation issues are not addressed here. To make the benefits of IMM modeling and amplitude information clearly visible, false detections (clutter, electronic counter measures), data association conflicts, or possibly unresolved measurements were excluded. Nevertheless, their impact might well be incorporated into the general Bayesian framework [16].

A. Sensor Modeling for Phased-array Radar

In phased-array radar tracking, additional sensor information can be acquired when needed. Before each “radar resource allocation” [7], certain radar parameters must be selected by the tracking system depending on the current lack of information. We here consider the *object revisit time* t_k , the current *beam position* \mathbf{b}_k , i.e. a unit vector pointing into the direction where radar energy is to be transmitted, and the transmitted *energy per dwell* e_k . Other radar parameters (detection threshold λ_D , radar beam width B) are assumed to be constant. After processing the skin echo produced by the illuminated object, the resource allocation R_k at time t_k results in measurements of direction cosines of the object and the object range, $\mathbf{z}_k =$

$(\bar{u}_k, \bar{v}_k, \bar{r}_k)$, along with the signal amplitude a_k . A single dwell may be insufficient for object detection and subsequent fine localization. Let n_{B_k} denote the number of dwells needed for a successful detection and $B_k = \{\mathbf{b}_k^i\}_{i=1}^{n_{B_k}}$ the set of the corresponding beam positions. Each radar allocation is thus characterized by the tuple $R_k = (t_k, B_k, n_{B_k}, e_k, \mathbf{z}_k, a_k)$. The sequence of successive allocations is denoted by $\mathcal{R}^k = \{R_k, \mathcal{R}^{k-1}\}$.

1) *Radar Cross Section Fluctuations*: The instantaneous radar cross section σ_k of realistic objects strongly depends on the radar frequency used and the current aspect angle. For this reason, statistical models are used for describing the backscattering properties of the objects. In many practical cases, σ_k is described by gamma-densities,

$$p(\sigma_k | \bar{\sigma}, m) = \mathcal{G}_m(\sigma_k; \bar{\sigma}, m) \quad (49)$$

$$= \frac{(m/\bar{\sigma})^m}{\Gamma(m)} \sigma_k^{m-1} e^{-\sigma_k m/\bar{\sigma}}. \quad (50)$$

In this equation $\bar{\sigma}$ denotes the mean RCS of the object that is usually unknown, but constant in time and characteristic of a certain class of objects, while the parameter m denotes the number of "degrees of freedom". The individual samples σ_k are assumed to be statistically independent for subsequent dwells (guaranteed by frequency decorrelation, e.g.). The cases $m = 1, 2$ are referred to as Swerling-I and -III fluctuations [11].

Let the instantaneous object signal $\mathbf{v}_k = (v_1, v_2)$ with the two orthogonal signal components v_1 and v_2 be additively corrupted by Gaussian noise with variance σ_n^2 according to the standard modeling assumptions [11]. Since the signal components are assumed to be statistically independent, the pdf of the resulting sensor signal $\mathbf{s}_k = (s_1, s_2)$ is

$$p(\mathbf{s}_k | \mathbf{v}_k) = \mathcal{N}(s_1; v_1, \sigma_n^2) \mathcal{N}(s_2; v_2, \sigma_n^2). \quad (51)$$

The normalized scalar quantity $a_k^2 = (s_1^2 + s_2^2)/2\sigma_n^2$, derived from \mathbf{s}_k , is thus Rice-distributed [11]: $p(a_k^2 | \text{sn}_k) = e^{-a_k^2 - \text{sn}_k} I_0(2a_k \sqrt{\text{sn}_k})$ with $\text{sn}_k = (v_1^2 + v_2^2)/2\sigma_n^2$. Hence, sn_k denotes the instantaneous signal-to-noise ratio of the object being proportional to the instantaneous radar cross section σ_k . The expectation value of a_k^2 with respect to $p(a_k^2 | \text{sn}_k)$ is given by $\mathbb{E}[a_k^2] = 1 + \text{sn}_k$. According to the normalization chosen, pure noise ($\text{sn}_k = 0$) has thus unit power. Due to the RCS model previously discussed, sn_k is gamma-distributed with the mean SN: $p(\text{sn}_k | \text{SN}) = \mathcal{G}_m(\text{sn}_k; \text{SN}, m)$. The conditional density of a_k^2 given SN is thus obtained by calculating:

$$p(a_k^2 | \text{SN}) = \int_0^\infty d\text{sn}_k p(a_k^2 | \text{sn}_k) p(\text{sn}_k | \text{SN}). \quad (52)$$

The integration can be carried out (see [1], e.g.) yielding:

$$p(a_k^2 | \text{SN}) = \left(\frac{m+\text{SN}}{m}\right)^{-m} e^{-ma_k^2/(m+\text{SN})} L_{m-1}\left(\frac{-a_k^2 \text{SN}}{m+\text{SN}}\right) \quad (53)$$

where L_{m-1} denotes the Laguerre polynomials. For Swerling-I/III these polynomials are given by: $L_0(-x) = 1$, $L_1(-x) = 1+x$. Obviously, $p(a_k^2 | \text{SN})$ can be interpreted as a gamma mixture with the expectation value $\mathbb{E}[a_k^2] = 1 + \text{SN}$.

2) *Mean Received Signal-to-Noise Ratio*: Any sensor model for phased-array radar tracking has to provide a functional relationship between the expected signal-to-noise ratio SN_k at the revisit time t_k , the sensor parameters considered (here: transmitted energy, beam position) and the relevant object parameters (mean RCS, object position). With a Gaussian beam form model [17], well proven in applications, the radar range equation (see [11], e.g.), we assume:

$$\text{SN}_k = \text{SN}_0 \left(\frac{\bar{\sigma}}{\bar{\sigma}_0}\right) \left(\frac{e_k}{e_0}\right) \left(\frac{r_k}{r_0}\right)^{-4} e^{-2\Delta b_k} \quad (54)$$

$$\text{with } \Delta b_k = |\mathbf{d}_k - \mathbf{b}_k|^2 / B^2. \quad (55)$$

r_k is the actual object range at time t_k , while $\mathbf{d}_k = (u_k, v_k)^\top$ denotes the related direction cosines. With the beam position $\mathbf{b}_k = (b_k^u, b_k^v)^\top$ and the (one-sided) beam width B , Δb_k is a measure of relative beam positioning error. The radar parameter SN_0 is the expected mean signal-to-noise ratio of a object with a standard mean cross section $\bar{\sigma}_0$ at a reference range r_0 that is directly ($\Delta b_k = 0$) illuminated by the beam with the energy e_0 . Due to the functional relationship stated in Equation 53, the signal strength a_k^2 can be interpreted as a measurement of $\bar{\sigma}$.

3) *Detection and Measurement Process*: A detection is assumed if the received signal strength exceeds a certain detection threshold: $a_k^2 > \lambda_D$. For a given m in the fluctuation model (Equation 50), the detection probability P_D is a function of SN and λ_D :

$$P_D(\text{SN}, \lambda_D, m) = \int_{\lambda_D}^{\infty} da_k^2 p(a_k^2 | \text{SN}). \quad (56)$$

The false alarm probability P_F is analogously obtained: $P_F(\lambda_D) = P_D(0, \lambda_D, m) = e^{-\lambda_D}$. Integration results in explicit expressions for P_D [11]. For Swerling-I/III fluctuations, we obtain:

$$P_D^I(\text{SN}, \lambda_D) = e^{-\frac{\lambda_D}{1+\text{SN}}} = P_F^{\frac{1}{1+\text{SN}}} \quad (57)$$

$$P_D^{III}(\text{SN}, \lambda_D) = e^{-\frac{\lambda_D}{1+\text{SN}/2}} \left(1 + \frac{(\text{SN}/2)\lambda_D}{(1+\text{SN}/2)^2}\right). \quad (58)$$

For object tracking a_k^2 is available after a detection, i.e. $a_k^2 > \lambda_D$. We thus need the conditional density:

$$p(a_k^2 | a_k^2 > \lambda_D, \text{SN}, m) = \begin{cases} \frac{p(a_k^2 | \text{SN})}{P_D(\text{SN}, \lambda_D, m)} & \text{for } a_k^2 > \lambda_D \\ 0 & \text{else} \end{cases}. \quad (59)$$

For strong objects we can assume $\text{SN} \approx 1 + \text{SN} \approx \dots \approx m + \text{SN}$ and thus approximately obtain: $p(a_k^2 | \text{SN}) \approx \left(\frac{\text{SN}}{m}\right)^{-m} e^{-ma_k^2/\text{SN}} L_{m-1}(-a_k^2)$, which is similar to the expression in Equation 53. On the other hand, let the detection probability for $m \neq 1$ be approximately given by: $P_D(\text{SN}, \lambda_D, m) \approx P_D^I(\text{SN}, \lambda_D)$ (i.e. by a Swerling-I-model). We can therefore write: $p(a | a_k^2 > \lambda_D, \text{SN}, m) \approx S_m(a_k^2; \text{SN}, m)$ with:

$$\mathcal{S}_m(a_k^2; \text{SN}, m) = \begin{cases} \left(\frac{\text{SN}}{m}\right)^{-m} e^{-(ma_k^2 + \lambda_D)/\text{SN}} L_{m-1}(-a_k^2) & \text{for } a_k^2 > \lambda_D \\ 0 & \text{else.} \end{cases} \quad (60)$$

Let us furthermore assume that monopulse localization after detection result in bias-free measurements u'_k, v'_k of the direction cosines and range with Gaussian measurement errors. According to [11], the standard deviations $\sigma_k^{u,v}$ depend on the beam width B and the instantaneous sn_k in the following manner: $\sigma_k^{u,v} \propto B/\sqrt{\text{sn}_k} \approx B/\sqrt{a_k^2 - 1}$. Since sn_k is unknown, in the last approximation a_k^2 is used as a bias-free estimate of sn_k ($\mathbb{E}[a_k^2] = 1 + \text{sn}_k$). The range error is assumed to be Gaussian with a constant standard deviation σ_r . Evidently, this model of the measurement process does not depend on the RCS fluctuation model.

B. Bayesian Tracking Algorithms Revisited

According to the previous discussion, object tracking is an iterative updating scheme for conditional probability densities $p(\mathbf{x}_k | \mathcal{R}^k)$ that describe the current object state \mathbf{x}_k given all available resource allocations \mathcal{R}^k and the underlying a priori information in terms of statistical models. The processing of each new measurement \mathbf{z}_k via Bayes' Rule establishes a recursive relation between the densities at two consecutive revisit times (a prediction step followed by filtering).

$$p(\mathbf{x}_k | \mathcal{R}^{k-1}) = \sum_{\mathbf{j}_k} p_{k|k-1}^{\mathbf{j}_k} \mathcal{N}(\mathbf{x}_k; \mathbf{x}_{k|k-1}^{\mathbf{j}_k}, \mathbf{P}_{k|k-1}^{\mathbf{j}_k}) \quad (61)$$

with $\mathbf{j}_k = (j_k, \dots, j_{k-n+1})$ denoting a particular *model history*, i.e. a sequence of possible hypotheses regarding the object dynamics model from a certain observation at time t_{k-n+1} up to the most recent measurement at time t_k ("n scans back"). In the case of a single dynamics model ($r = 1$), the prediction densities $p(\mathbf{x}_k | \mathcal{R}^{k-1})$ are strictly given by Gaussians (standard Kalman prediction). For $n = 1$, $p(\mathbf{x}_k | \mathcal{R}^{k-1})$ is approximated by a mixture with r components according to the r dynamics models used. GPB2 and standard IMM algorithms are possible realizations of this scheme [3]. For standard IMM, the approximations are made after the prediction, but before the filtering step, while for GPB2 they are applied after the filtering step. Hence, GPB2 requires more computational effort. For details see [3].

2) *Processing of Signal Strength Information*: Let us treat the normalized mean RCS of the object, $s_k = \bar{\sigma}_k / \bar{\sigma}_0$, as an additional component of the state vector. Since the signal strength after a detection occurred may be viewed as a measurement of s_k , let us consider the augmented conditional density

$$p(\mathbf{x}_k, s_k | \mathcal{R}^k) = p(s_k | \mathbf{x}_k, \mathcal{R}^k) p(\mathbf{x}_k | \mathcal{R}^k). \quad (62)$$

The calculation of $p(\mathbf{x}_k | \mathcal{R}^k)$ was discussed in section 2. For the remaining density $p(s_k | \mathbf{x}_k, \mathcal{R}^k)$, an application of Bayes' Rule yields up to a normalizing constant:

$$p(s_k | \mathbf{x}_k, a_k^2, \mathcal{R}^{k-1}) \propto \mathcal{S}_m(a_k^2; \text{SN}, m) p(s_k | x_k, R^{k-1}). \quad (63)$$

Let us furthermore assume that $p(s_k | \mathbf{x}_k, \mathcal{R}^{k-1})$ are given by inverse gamma densities,

$$p(s_k | \mathbf{x}_k, \mathcal{R}^{k-1}) = \mathcal{I}_{\mu_{k|k-1}}(s_k; \hat{s}_{k|k-1}, \mu_{k|k-1}), \quad (64)$$

which are defined by:

$$\mathcal{I}_{\mu}(s; \hat{s}, \mu) = [((\mu - 1)\hat{s})^{\mu} / \Gamma(\mu)] s^{-\mu-1} e^{-\frac{(\mu-1)\hat{s}}{s}}, \quad (65)$$

where \hat{s} is the expectation of this density, $\hat{s} = \mathbb{E}[s] > 0$, μ a parameter $\mu > 1$. For $\mu > 2$, the related variance exists: $\mathbb{V}[s] = \hat{s}^2 / (\mu - 2)$. This class of densities is invariant under the successive application of Bayes Rule according to Equation 63, since up to normalization we obtain:

$$\mathcal{S}_m(a_k^2; \text{SN}, m) \mathcal{I}_{\mu_{k|k-1}}(s_k; \hat{s}_{k|k-1}, \mu_{k|k-1}) \quad (66)$$

$$\propto \alpha_k^{-m} s_k^{-\mu_{k|k-1}-m-1} \exp\left(-\frac{(\mu_{k|k-1}-1)\hat{s}_{k|k-1} + \frac{ma_k^2 + \lambda_D}{\alpha_k}}{s_k}\right) \quad (67)$$

$$\propto \mathcal{I}_{\mu_k}(s_k; \hat{s}_k, \mu_k), \quad (68)$$

where the parameters α_k , \hat{s}_k and μ_k are given by:

$$\alpha_k = \text{SN}_0 \left(\frac{e_k}{e_0}\right) \left(\frac{r_k}{r_0}\right)^{-4} e^{-2\Delta b_k}, \quad (69)$$

$$\hat{s}_k = \frac{\mu_{k|k-1}-1}{\mu_{k|k-1}+m-1} \hat{s}_{k|k-1} + \frac{(ma_k^2 + \lambda_D)/\alpha_k}{\mu_{k|k-1}+m-1} \quad (70)$$

$$\mu_k = \mu_{k|k-1} + m. \quad (71)$$

With reference to s_k the density $\mathcal{I}_{\mu_k}(s_k; \hat{s}_k, \mu_k)$ is correctly normalized. Evidently, α_k depends on the object position ($\alpha_k = \alpha_k(r_k, u_k, v_k)$). In order to preserve the factorization of $p(\mathbf{x}_k | s_k, \mathcal{R}^k)$ in a normal mixture related to the kinematic properties of the object \mathbf{x}_k and an inverse gamma density related to its RCS s_k , we use the approximation:

$$\alpha_k \approx \left(\frac{e_k}{e_0}\right) \left(\frac{\hat{r}_k}{r_0}\right)^{-4} e^{-2\{(\hat{u}_k - b_k^u)^2 + (\hat{v}_k - b_k^v)^2\}/B^2}, \quad (72)$$

where \hat{r}_k , \hat{u}_k , \hat{v}_k are the MMSE estimates for r_k , u_k and v_k derived from $p(\mathbf{x}_k | \mathcal{R}^k)$. Hence, α_k compensates both the estimated positioning error of the radar beam and the propagation loss due to the radar equation. Assuming s_k to be constant, we have $\mathcal{I}_{\mu_{k|k}}(s_k; \hat{s}_{k|k-1}, \mu_{k|k}) = \mathcal{I}_{\mu_{k|k-1}}(s_k; \hat{s}_{k-1}, \mu_{k|k-1})$. In principle, a dynamics model describing temporal changes of the radar cross section might be introduced.

C. Adaptive Bayesian Sensor Management

The tracking results are essential for adaptive radar revisit time control, the selection of the transmitted radar energy, and the design of intelligent algorithms for local search.

1) *Adaptive Radar Revisit Time Control*: The time t_k when a radar allocation R_k should take place is determined by the current lack of information conveniently described [17] by the error covariance matrix $\mathbf{P}_{k|k-1}$ of the predicted state estimate $\mathbf{x}_{k|k-1}$. Since $p(\mathbf{x}_k | \mathcal{R}_{k-1})$ is a normal mixture, $\mathbf{x}_{k|k-1}$ and $\mathbf{P}_{k|k-1}$ are given by:

$$\mathbf{x}_{k|k-1} = \sum_{\mathbf{j}_k} p_{k|k-1}^{\mathbf{j}_k} \mathbf{x}_{k|k-1}^{\mathbf{j}_k} \quad (73)$$

$$\mathbf{P}_{k|k-1} = \sum_{\mathbf{j}_k} p_{k|k-1}^{\mathbf{j}_k} (\mathbf{P}_{k|k-1}^{\mathbf{j}_k} + (\mathbf{x}_{k|k-1}^{\mathbf{j}_k} - \mathbf{x}_{k|k-1})(\mathbf{x}_{k|k-1}^{\mathbf{j}_k} - \mathbf{x}_{k|k-1})^\top). \quad (74)$$

The covariance matrix $\mathbf{P}_{k|k-1}^{\mathbf{j}_k}$ of the individual mixture components grow the faster in time the more often maneuvers are assumed in the corresponding model histories. This has an impact on the total covariance matrix $\mathbf{P}_{k|k-1}$ according to the corresponding weighting factors $p_{k|k-1}^{\mathbf{j}_k}$. In addition, $\mathbf{P}_{k|k-1}$ is "broadened" by the positively definite spread terms $(\mathbf{x}_{k|k-1}^{\mathbf{j}_k} - \mathbf{x}_{k|k-1})(\mathbf{x}_{k|k-1}^{\mathbf{j}_k} - \mathbf{x}_{k|k-1})^\top$. Obviously, the adaptive IMM modeling affects $\mathbf{P}_{k|k-1}$ in a rather complicated way.

A scalar measure of the information deficit is provided, e.g., by the largest eigenvalue of the covariance matrix of the predicted object direction (in terms of u, v). Let it be denoted by $G_{k|k-1}$. A track update is allocated when the $G_{k|k-1}$ exceeds a predetermined proportion of the squared radar beam width B :

$$G_{k|k-1} > (v_0 B)^2. \quad (75)$$

The *relative track accuracy* v_0 introduced by this criterion is a measure of the minimum track quality required and a parameter to be optimized. In many practical applications, $v_0 = 0.3$ is a reasonable choice [17].

2) *Transmitted Radar Energy Selection*: In view of the tracking system, the sensor performance is mainly characterized by the signal-to-noise ratio that determines both, the detection probability and the measurement error. By suitably choosing the transmitted energy per dwell e_k , the expected signal-to-noise ratio $\text{SN}_{k|k-1}$ can be kept constant during tracking. Besides v_0 , $\text{SN}_{k|k-1}$ is an additional parameter subject to optimization. Since v_0 may be viewed as a measure of the beam positioning error, the energy e_k at time t_k is defined by this condition (Equation 54):

$$\text{SN}_{k|k-1} \stackrel{!}{=} \text{const.} \quad (76)$$

$$\rightarrow \frac{e_k}{e_0} = \left(\frac{\text{SN}_0}{\text{SN}_{k|k-1}} \right) \left(\frac{\bar{\sigma}_0}{\bar{\sigma}} \right) \left(\frac{\hat{r}_{k|k-1}}{r_0} \right)^4 e^{2v_0^2}. \quad (77)$$

By this particular choice, the influence of the radar range equation is compensated (at least for a certain range interval). For the mean radar cross section $\bar{\sigma}$ either a worst-case assumption or estimates from object amplitude information can be used. The track quality v_0 also affects the transmitted energy. As a side effect of this choice, the standard deviations $\sigma_k^{u,v}$ of the u, v -measurements are kept constant on an average.

3) *Bayesian Local Search Procedures*: Intelligent algorithms for beam positioning and local search are crucial for IMM-type phased-array tracking. Overly simple strategies may easily destroy the benefits of the adaptive dynamics model, because track loss immediately after a model switch can easily occur. To avoid this phenomenon, we adapt the optimal approach based on the predicted densities $p(\mathbf{x}_k | \mathcal{R}^{k-1})$ proposed in [17] to IMM tracking [24].

1. The beam position \mathbf{b}_k^1 of the first dwell at time t_k is simply given by the predicted direction $\mathbf{d}_{k|k-1}$ to be derived from the predicted density function $p(\mathbf{x}_k | \mathcal{R}^{k-1})$.
2. If no detection occurs in the first dwell, this very result provides useful information on the target. We thus have to calculate the conditional density of the target state given the event $\neg D_k^1$: 'no detection at time t_k in the direction \mathbf{b}_k^1 '.
3. An application of Bayes' Rule directly yields:

$$p(\mathbf{d}_k | \neg D_k^1, \mathcal{R}^{k-1}) \propto (1 - P_D(\mathbf{d}_k; \mathbf{b}_k^1)) p(\mathbf{d}_k | \mathcal{R}^{k-1}) \quad (78)$$

up to a normalizing factor. In this expression, the detection probability P_D depends on the expected SN (Equation 54) and thus on the current beam and target position $\mathbf{b}_k, \mathbf{d}_k$.

4. The two dimensional density $p(\mathbf{d}_k | \neg D_k^1, \mathcal{R}^{k-1})$ can easily be calculated on a grid. The beam position for the next dwell is then simply provided by its maximum.
5. This computational scheme for Bayesian local search is repeated until a detection occurs. Since the maximum of the densities $p(\mathbf{d}_k | \neg D_k^1, \neg D_k^2, \dots, \mathcal{R}^{k-1})$ is searched, the computation of the normalization integral is not required. Numerically efficient realizations are possible.

Alternatively, $p(\mathbf{d}_k | \neg D_k^1, \mathcal{R}^{k-1})$ might be used for calculating the expected SN in a certain direction \mathbf{b}_k :

$$\text{SN}(\mathbf{b}_k) = \int d\mathbf{d}_k \text{SN}(\mathbf{b}_k, \mathbf{d}_k) p(\mathbf{d}_k | \neg D_k^1, \mathcal{R}^{k-1}).$$

Searching the maximum of $\text{SN}(\mathbf{b}_k)$ results in a different local search strategy. In the examples considered below, however, no significant performance improvements were observed. Nevertheless, there might be applications where the maximization of $\text{SN}(\mathbf{b}_k)$ is advantageous (e.g. for track recovery in case of intermittent operating modes).

This local search scheme exploits 'negative' evidence, as also here the lack of an expected measurement carries information on the current target position. We here in particular observe a direct impact on adaptive sensor management. Again, the prerequisite for dealing with negative evidence is an adequate sensor performance model. As in the case of resolution phenomena (section 2), the processing of negative sensor evidence implies mixture densities with possibly *negative* mixture coefficients, i.e. not each mixture component has a direct probabilistic interpretation. As the mixture coefficients sum up to one, the overall density nevertheless has a well-defined probabilistic meaning.

Figure 4 illustrates this scheme of Bayesian local search for a particular example. In Figure 4a the predicted pdf $p(\mathbf{d}_k | \mathcal{R}^{k-1})$, a mixture density, is shown for some time t_k . The target is expected to be in the bright region with high probability, the true target position being indicated by a green dot. The blue dot denotes the beam position of the next dwell. The related detection probability is 26%. However, no detection occurred during the first dwell

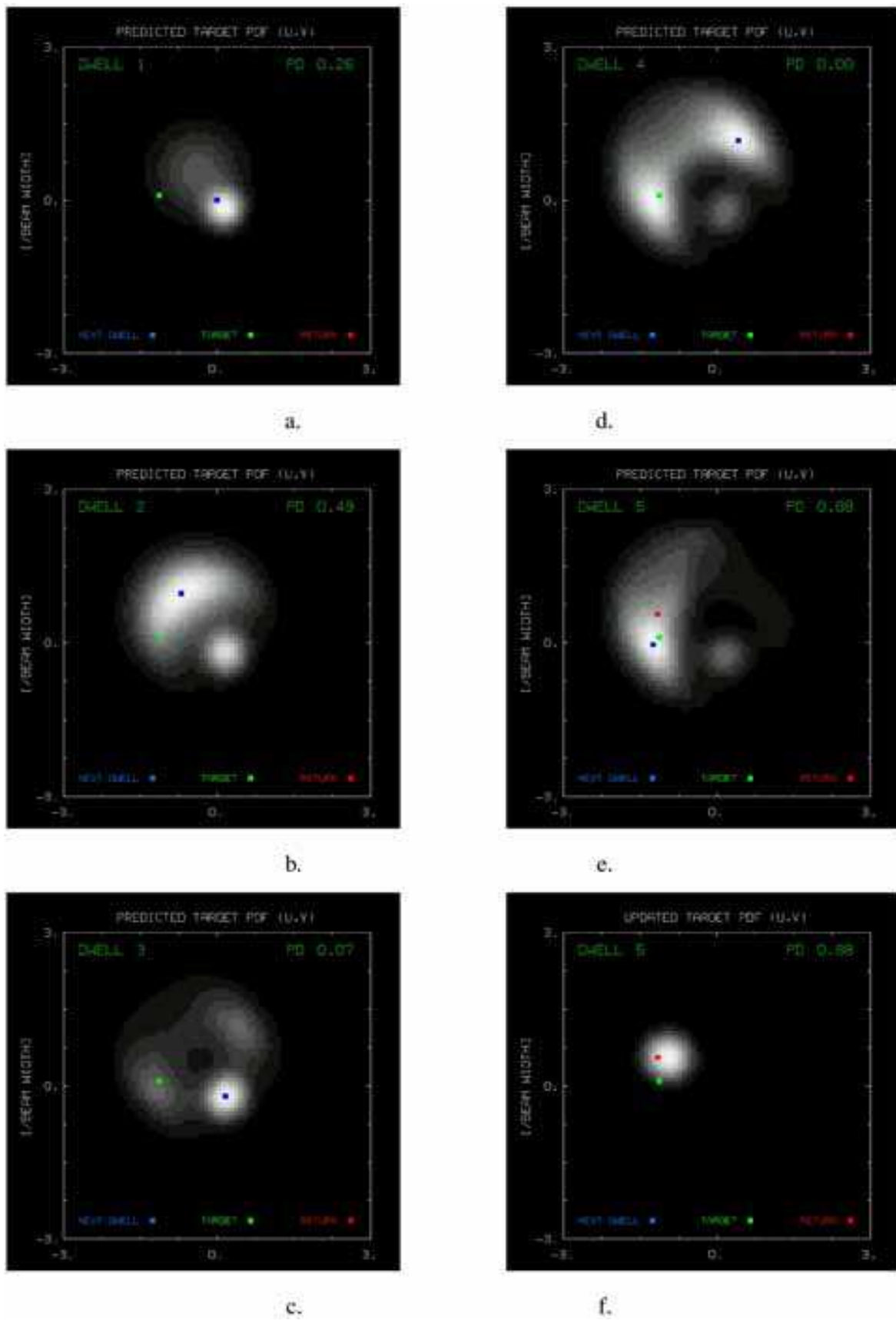


Fig. 4. Bayesian local search: five consecutive dwells

1. We thus calculate the conditional pdf $p(\mathbf{d}_k | \neg D_k^1, \mathcal{R}^{k-1})$ given that event. As visible in Figure 4b, it differs significantly from $p(\mathbf{d}_k | \mathcal{R}^{k-1})$. The previous maximum decreased in height, while the global maximum is at a different location. Again no detection occurred; the resulting density $p(\mathbf{d}_k | \neg D_k^1, \neg D_k^2, \mathcal{R}^{k-1})$ reflecting the two pieces of ‘negative’ evidence $\neg D_k^1$ and $\neg D_k^2$ is shown in Figure 4c. Now the search algorithm decides to look again near the position at dwell 1. Although wrong in this case, this does not seem to be unreasonable. In addition, two smaller local maxima appear that increase in size as in the next dwell also no detection occurred. According to Figure 4d the next decision is ambiguous. We finally obtain a decision which leads to success. The last picture shows the updated pdf (Figure 4f).

4. Discussion of numerical simulation results

Simulation results provide hints as to what extent the total performance of multiple-object air surveillance by phased-array can be improved by using adaptive techniques for combined tracking and sensor control. The following four questions are addressed:

1. What resource savings (allocation time, energy) can be expected by using adaptive dynamics models?
2. How should the IMM dynamics modeling be designed (e.g. number of models, transition matrix)?
3. What energy savings can be expected by exploiting object amplitude information for sensor control?
4. Why is Bayesian local search important when adaptive dynamics models are used for revisit time control?

A. Discussion of Simulation Scenarios

In general we follow the parameter and threshold settings recommended in [17]. To exclude false alarms due to receiver noise, the false alarm probability is $P_F = 10^{-4}$. False returns due to clutter or ECM are not considered. The standard deviation of the measurement errors in object range is $\sigma_r = 100$ m, while the the radar beam width is $B = 1^\circ$. We assume a minimum time interval of 20 ms between consecutive dwells on a particular object and statistically independent signal amplitudes (frequency decorrelation, e.g.). The reference range is set to $r_0 = 80$ km.

1) *IMM Modeling Parameters:* Antenna coordinates (direction cosines, range) are used also for tracking; non-linearities introduced by these non-Cartesian coordinates are taken into account [16]. In each component u_k, v_k, r_k the state vector is given by position, speed, and acceleration. For the sake of simplicity, we consider a block diagonal system matrix defined by

$$\mathbf{F}_{k|k-1} = \begin{pmatrix} 1 & \Delta t_k \mathbf{1} & \frac{1}{2} \Delta t_k^2 \mathbf{1} \\ \mathbf{0} & 1 & \Delta t_k \mathbf{1} \\ \mathbf{0} & \mathbf{0} & e^{-\Delta t_k / \theta} \end{pmatrix} \quad (79)$$

$$\mathbf{D}_{k|k-1} = \Sigma^2 (1 - e^{-2\Delta t_k / \theta}) \begin{pmatrix} \mathbf{0} & \mathbf{0} & \mathbf{0} \\ \mathbf{0} & \mathbf{0} & \mathbf{0} \\ \mathbf{0} & \mathbf{0} & 1 \end{pmatrix}, \quad (80)$$

with $\Delta t_k = t_k - t_{k-1}$. The maneuvering capability of the objects is thus characterized by two parameters: *maneuver correlation time* θ and *acceleration width* Σ . For $r = 2, 3$ we consider the parameter sets:

- M_1 (worst-case model): $\Sigma_1 = 60 \text{ m/s}^2$, $\theta_1 = 30 \text{ s}$
- M_2 (best-case model): $\Sigma_2 = 1 \text{ m/s}^2$, $\theta_2 = 10 \text{ s}$
- M_3 (medium-case model): $\Sigma_3 = 30 \text{ m/s}^2$, $\theta_3 = 30 \text{ s}$

The matrices of the model transition probabilities are given by:

$$(p_{ij})_{i=1,j=1}^2 = \begin{pmatrix} .8 & .1 \\ .2 & .9 \end{pmatrix}, \quad (p_{ij})_{i=1,j=1}^3 = \begin{pmatrix} .8 & .1 & .0 \\ .0 & .9 & .2 \\ .2 & .0 & .8 \end{pmatrix}. \quad (81)$$

We observed that the performance does not critically depend on the particular switching probabilities p_{ij} chosen. A detailed mismatch analysis, however, has not been performed. A track is considered to be lost if more than 50 dwells occur in the local search of if the beam positioning error Δb_k is greater than $3B$. We thus permit even a rather extensive local search that correspondingly burdens the total energy budget. In all simulations considered below (1000 runs) the relative frequency of track loss is less than 2%.

2) *Selected Benchmark Trajectories*: The horizontal projection of four standard benchmark trajectories (military cargo aircraft, medium bomber, fighter/attack aircraft, and anti-ship missile) is shown in Figure 5 along with representative kinematical characteristics such as acceleration (solid line), range (dashed), height (dotted), and speed (solid). They have been proposed in [8], [9] and cover a rather wide range of militarily relevant objects. The missile trajectory might serve to explore the performance limits of the algorithms. In principle, missiles can execute even stronger maneuvers. It is questionable, however, if for those objects and their individual missions the dynamics models discussed above remain applicable. All objects are tracked over a period of 180 s. The RCS fluctuations are described by a Swerling-III model. The mean cross sections significantly vary from object to object (4., 2., 1.2, .5 m²).

3) *Measures of Performance Considered*: The discussion is confined to a few intuitively clear and simple performance measures obtained by Monte-Carlo simulation (1000 runs). In general a single performance measure is not sufficient as there may exist applications where the transmitted energy is the limiting factor, while in a different scenario the number of radar allocations must be kept low.

The adaptivity becomes visible if the performance is evaluated as a function of the tracking time that can be compared with the kinematics of the individual trajectories (Figure 5). Here we used histograms with 100 cells. In particular we considered: the mean revisit intervals, the mean number of dwells for a successful update, the mean number of sensor allocations in total required for track maintenance, the mean energy spent for a successful allocation, the mean energy totally spent for track maintenance, and the mean RCS of the objects estimated during tracking.

Four tracking filters were compared: worst-case Kalman filter (KF), standard IMM filter with two or three models, respectively (S-IMM_{2,3}), and IMM-MHT filtering with model histories of length $n = 4$. For IMM-MHT with $n > 4$, the performance characteristics change only slightly. We thus conclude that $n = 4$ already provides a good approximation to optimal filtering (at least for the scenarios considered here). With reference to object amplitude information we considered three cases: 1) the object RCS $\bar{\sigma}$ is known and used for energy management. 2) The mean RCS $\bar{\sigma}$ is unknown and to be estimated during tracking. 3) A worst-case assumption is used for all objects ($\bar{\sigma} = 0.5 \text{ m}^2$).

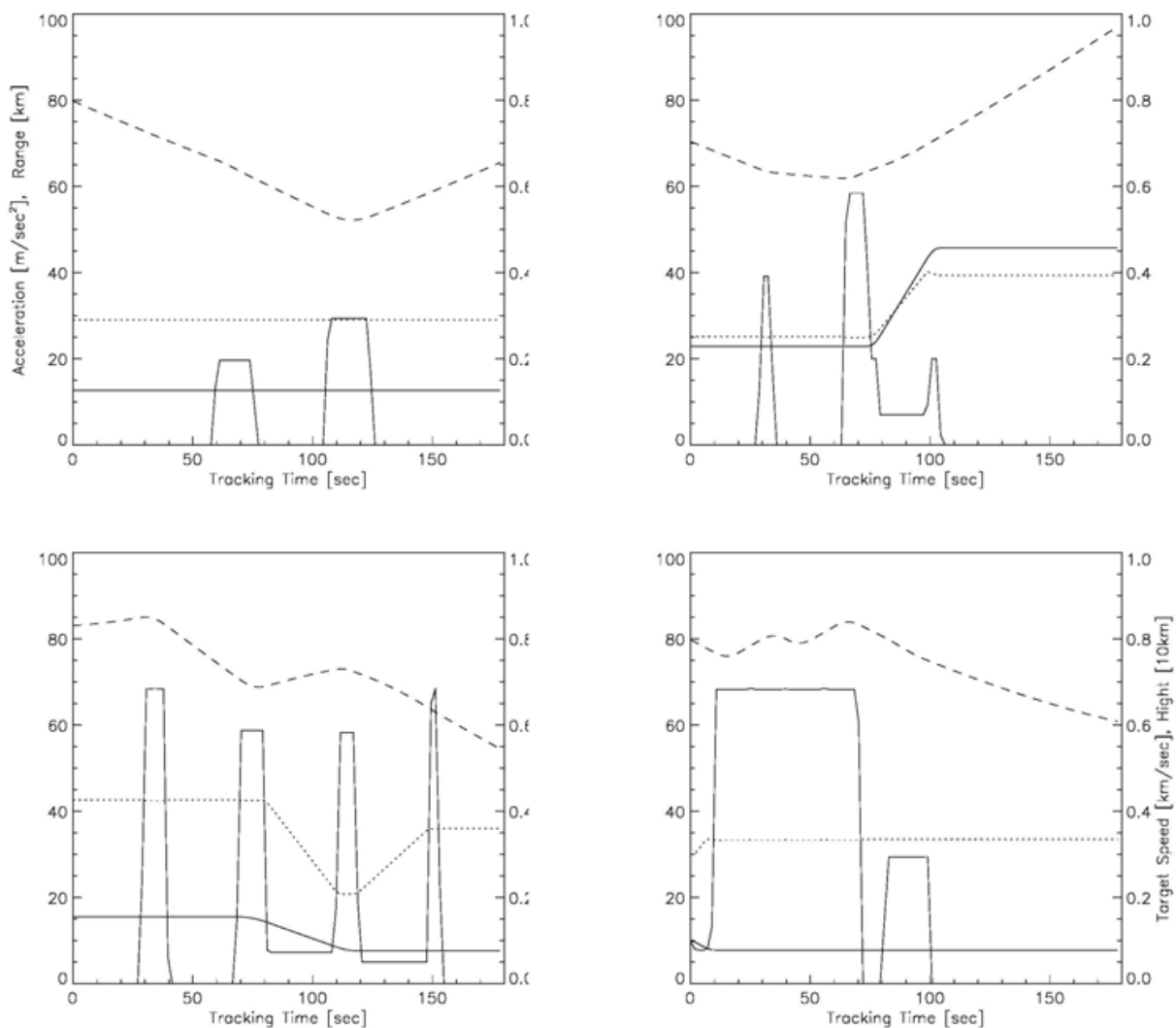


Fig. 5. Horizontal projections and kinematical quantities (military cargo aircraft, medium bomber, fighter/attack aircraft, and anti-ship missile)

B. Remarks on IMM Modeling Design

Practically, the question arises how many models should be used in the IMM approach. In addition it must be clarified if each trajectory needs an individual modelling or if the same IMM modelling can be used without significant loss of performance. For the fighter scenario, a worst/best-case model should be appropriate at first sight. Trajectory 1 (Cargo Aircraft), however, shows that military objects can occur for which medium-case models are sufficient. To answer these questions, we used IMM with two ($r = 2, M_1, M_2$) and three models ($r = 3, M_1, M_2, M_3$), respectively, with $v_0 = 0.3$, $SN_k|_{k-1} = 50$. How these parameters affect the performance is discussed further below. Figure 6 shows the resulting mean revisit intervals for all trajectories. The kinematical object characteristics are clearly mirrored. We observed:

1. As expected, Kalman filtering ($r = 1, M_1$) leads to constant revisit intervals that are comparable for all trajectories. This is no longer true for S-IMM. The resultant curves related to $r = 2$ (solid) and $r = 3$ (dashed) significantly differ from each other. The onset of maneuvers (Figure 5) strongly affects the mean update intervals and thus illustrates the adaptivity of the algorithm.

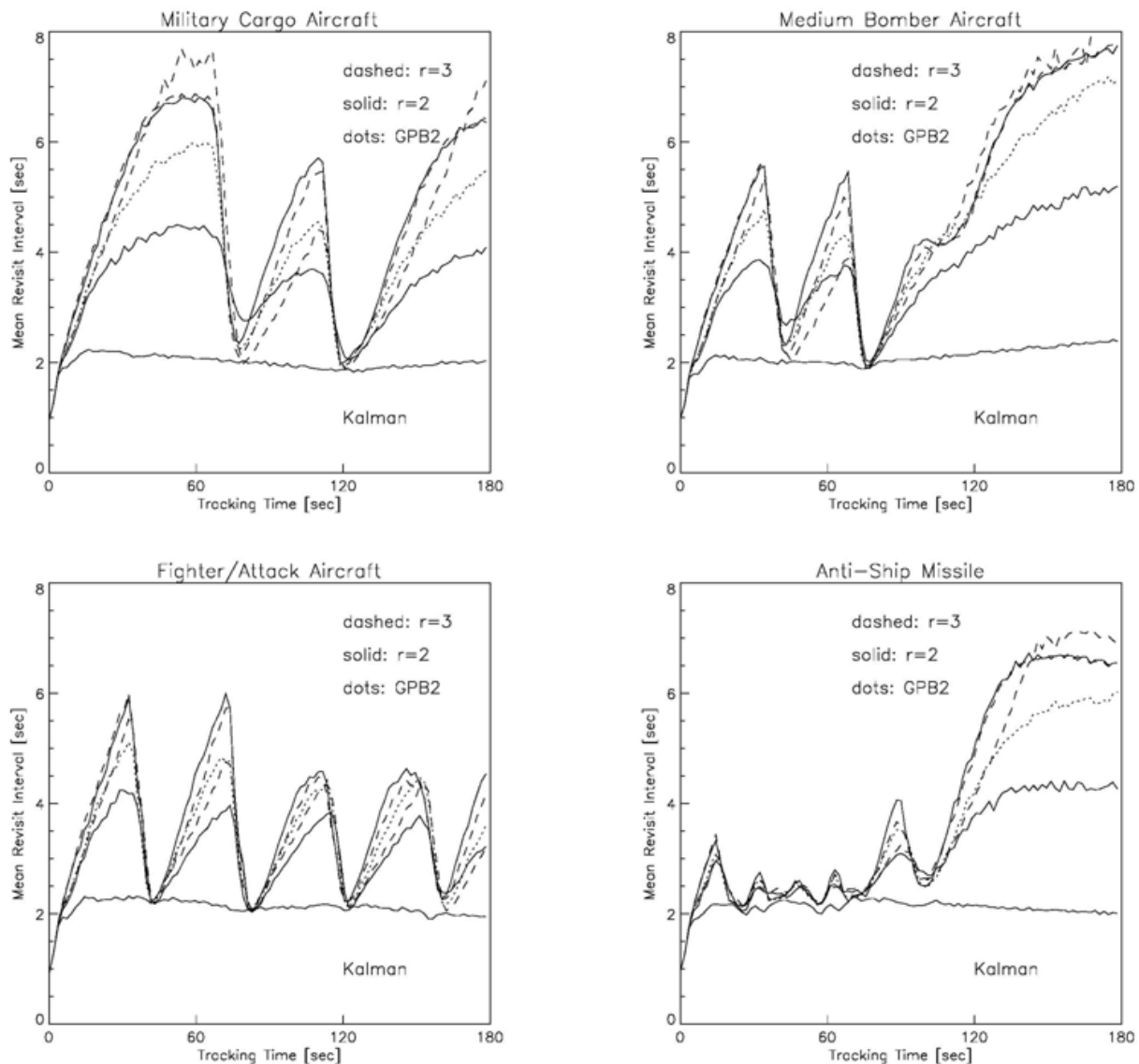


Fig. 6. Revisit intervals for different filters: military cargo aircraft, medium bomber, fighter/attack aircraft, and anti-ship missile

2. The difference between the cases $r = 2, 3$ vanishes however, if IMM-MHT is used. If model histories are permitted (here $n = 4$), it seems to be irrelevant if besides worst/bestcase assumption additional medium-case models are used. Even longer histories or further models ($r > 3$) do not significantly improve the performance obtained with $r = 2$ and $n = 4$. For a suitable (!) choice of the switching probabilities, the performance of S-IMM₄ approaches closes to B-IMM₂; for B-IMM₄ no improvement over B-IMM₂ was observed.
3. For the bomber and the fighter, S-IMM₃ (M_1, M_2, M_3) outperforms S-IMM₂ (M_1, M_2), in spite of the fact that for these trajectories only worst-case maneuvers occur and the medium-case model appeared to be unnecessary at first sight. The difference between $r = 2$ and $r = 3$, however, is not as clear as for scenario 1 (cargo aircraft).
4. For the moderately maneuvering cargo aircraft, the question arises whether the performance can be improved by using a medium/best-case IMM modelling. We found

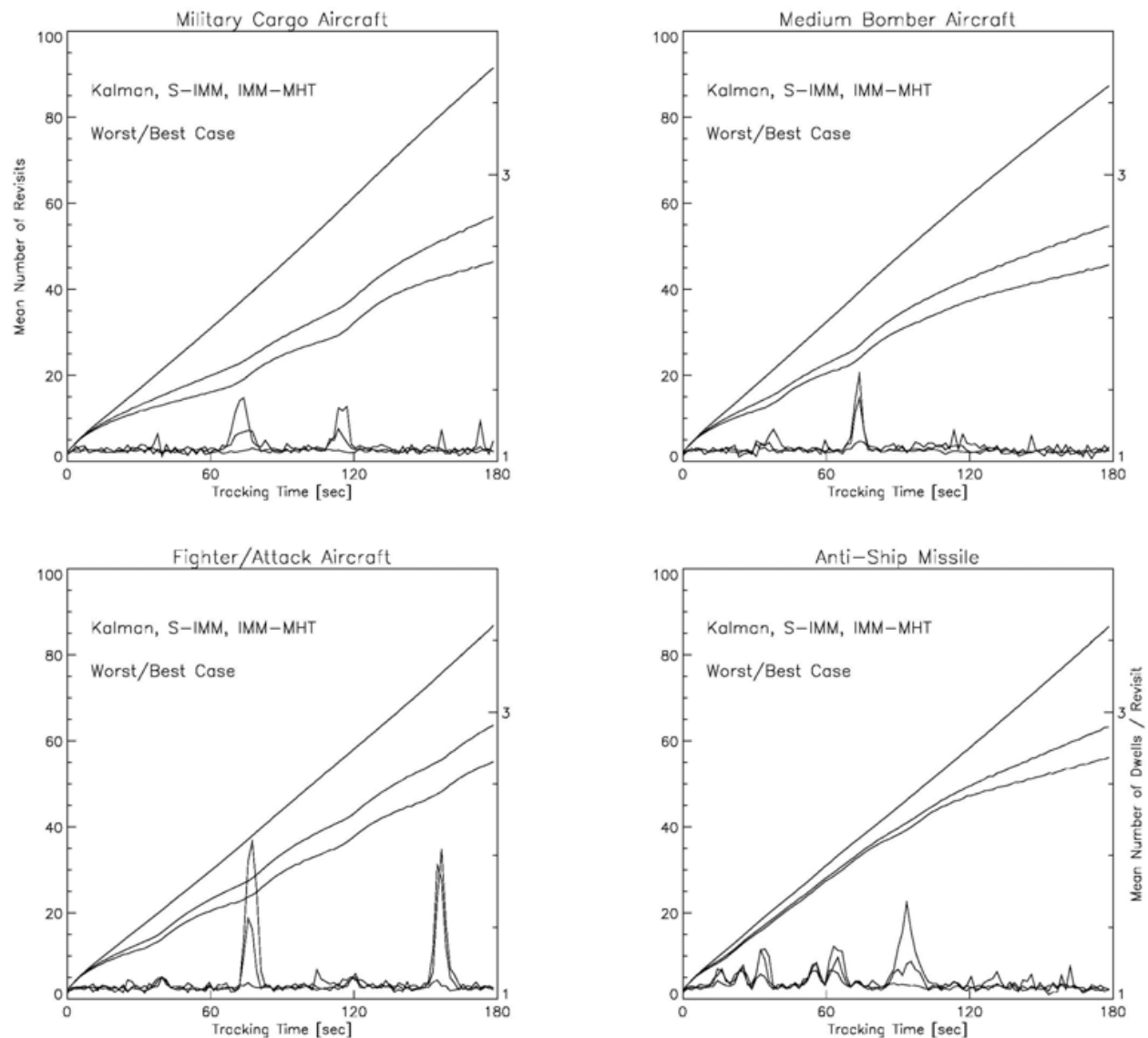


Fig. 7. Radar allocations for different filters: military cargo aircraft, medium bomber, fighter/attack aircraft, and anti-ship missile

that worst/best-case IMM-MHT and medium/best-case IMM-MHT differ, but not very much. This indicates that worst/best-case IMM-MHT has a more or less “universal” character, i.e. it does not critically depend of the scenario considered (at least within certain limits).

These observations indicate that the mixtures $p(\mathbf{x}_k | \mathcal{R}^k)$ for $n = 4$, $r = 2$ have enough internal degrees of freedom to provide an adequate representation of the actual object behavior. Refined approximations by even more mixture components seem to be irrelevant for the trajectories considered. A rule of thumb: A worst/best-case analysis of the problem along with IMM-MHT seems to be sufficient to achieve a nearly optimal tracking performance. Obviously, for two dynamics models, reasonable and intuitive assumptions for the switching probabilities are easily obtained. IMM-MHT thus enables a more simplified dynamics modelling without significant loss of performance.

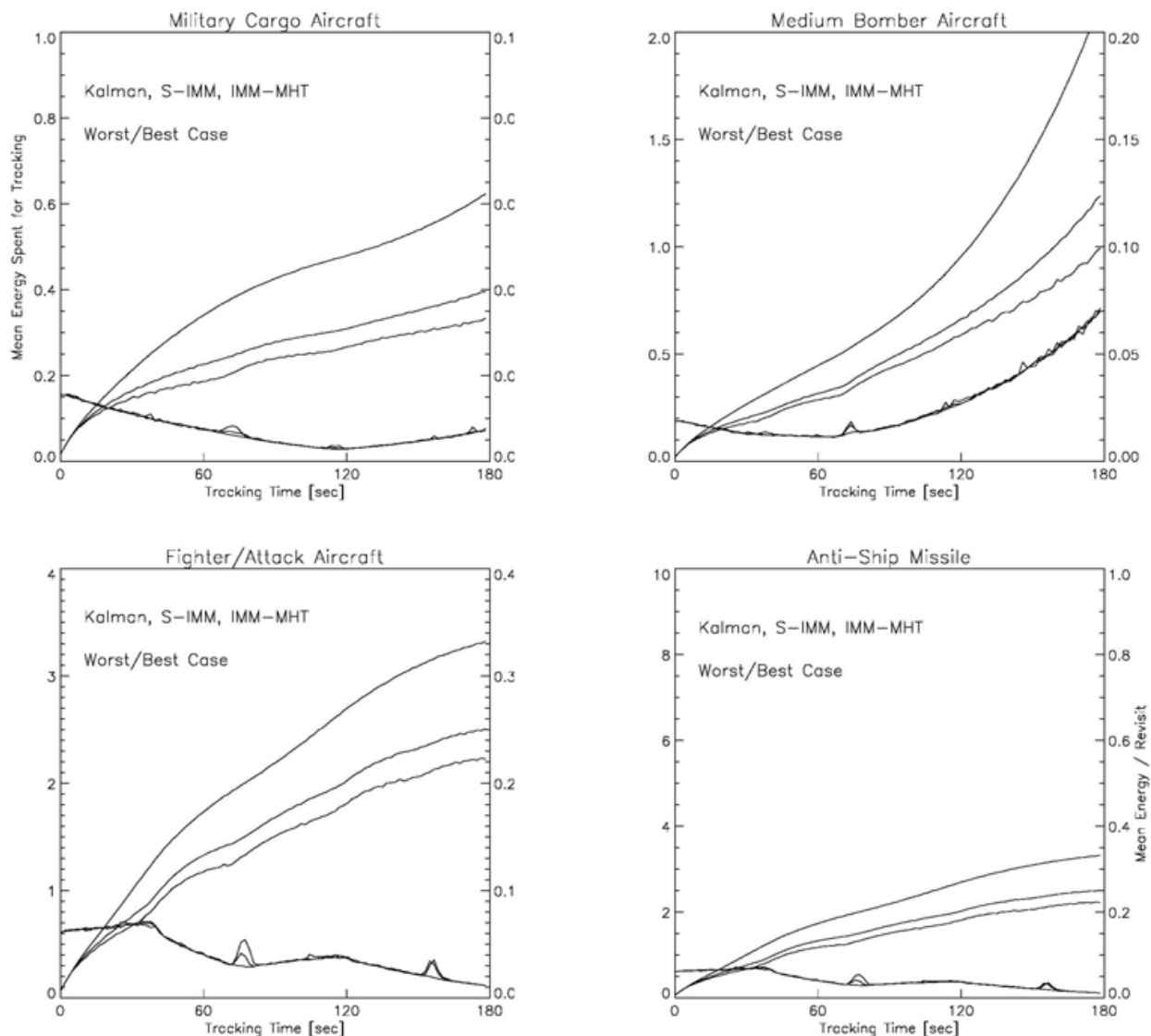


Fig. 8. Radar energy spent for different filters: military cargo aircraft, medium bomber, fighter/attack aircraft, and anti-ship missile

C. Gain by IMM Modelling

To investigate the gain by adaptive dynamics models, let us for the present assume that the mean RCS of the object is known and used for energy management. Figure 7 shows the mean number of allocations required for track maintenance (KF, S-IMM₂, B-IMM₂). As expected, for KF the mean number of revisits linearly increases with increasing tracking time and is nearly the same for all trajectories. By adaptive dynamics modeling, however, the number of sensor allocations is reduced.

1. Compared with KF, IMM results in significant resource savings. There is an improvement by IMM-MHT over S-IMM; the difference, however, is less significant than between SIMM and KF. Besides simplified modeling assumptions, the practical use of IMM-MHT therefore consists in the exploration of the limiting bounds for performance improvements.
2. The largest gain is observed for the cargo aircraft and the bomber. In the case of the fighter aircraft, the allocations required are reduced by about 50 % compared with

worstcase Kalman filtering. Even during the 7 *g* weaving of the missile, some advantages of the IMM modeling can be observed.

Figure 7 shows the mean number of dwells per revisit. Up to peaks corresponding with the onset of maneuvers, it is constant and roughly equal for all filters and trajectories. The more adaptive the filter is, the higher the peaks are, i.e. the larger the revisit intervals can be during inertial flight. The peaks thus indicate that for abrupt maneuvers a local search might be required. This is the price to be paid for increased adaptivity. Evidently, intelligent algorithms for beam positioning and local search are essential for IMM phased-array tracking. These observations are consistent with Figure 8, which shows the mean energy spent for track maintenance (relative units). Besides the object maneuvers, these curves are influenced by the current object range (Figure 5, dotted line). In addition, the mean energy spent per revisit is displayed. Up to characteristic peaks, the energy per revisit is roughly the same for all tracking filters.

D. On the Quality of RCS Estimates

In a practical application, the mean RCS of the objects to be tracked is unknown and might be estimated from object amplitude information. In general, the estimators used should be at least approximately bias-free, the estimated error and the empirical error should be roughly identical, and the estimators should show a certain robustness against model mismatch. As indicated by Figure 9, the estimator previously proposed provides rather satisfying results for all trajectories. Using IMM-MHT for tracking, the recursion was initiated with $\bar{\sigma} = .5 \text{ m}^2$ (worst-case assumption) and $m_0 = 1.01$.

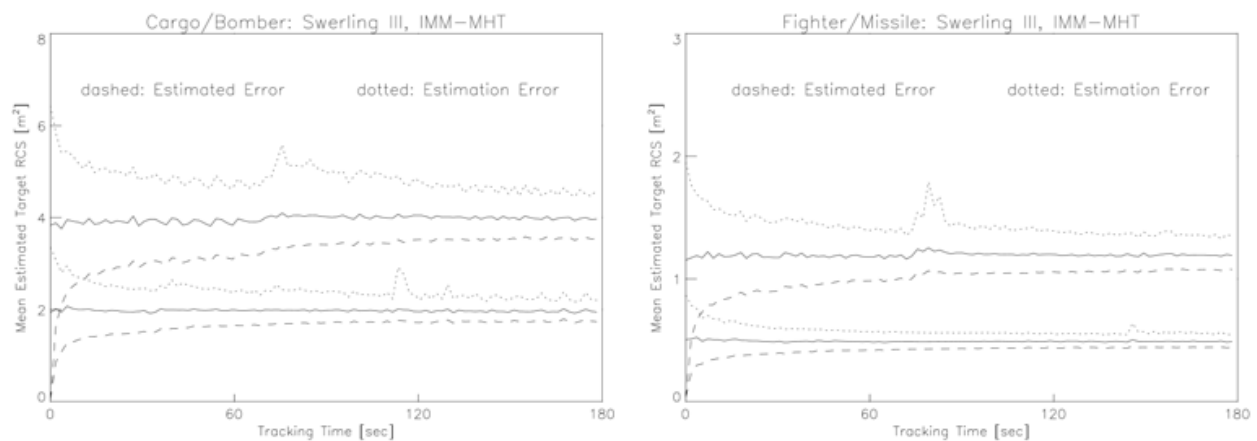


Fig. 9. On the quality of RCS estimates

The solid lines show the mean RCS estimates as a function of the tracking time. For all scenarios it is roughly constant and corresponds with the actual values (4, 2, 1.2, 0.5 m^2). The dotted lines indicate the mean estimation error (available in the simulation). The curves show peaks that are related to the onset of maneuvers and the corresponding lack of track accuracy. The dashed lines denote the mean standard deviation calculated by the estimator itself. Tracking and RCS estimation are closely interrelated: Only when tracked over a certain period of time, are estimates reliable enough to distinguish between the object classes. A satisfying RCS estimation by signal processing only, i.e. without a temporal integration along the estimated trajectory does not seem to be possible. In this context, IMM retrodiction techniques [23] might be considered that can provide more accurate estimates of the trajectory and thus more accurate RCS estimates.

object type	processed	simulated	RCS [m ²]	estimated error	estimation error	energy
Bomber	III	III	1.96	0.22	0.28	0.37
	III	I	2.34	0.25	0.57	0.42
	I	III	1.77	0.28	0.33	0.39
	I	I	2.03	0.32	0.34	0.44
Fighter	III	III	1.19	0.13	0.16	0.82
	III	I	1.41	0.15	0.34	1.
	I	III	1.07	0.16	0.19	0.86
	I	I	1.22	0.18	0.19	0.99

Table I. Mismatch regarding the fluctuation model

E. RCS Model Mismatch

The backscattering properties of real objects are highly complex. A practicable method for estimating the RCS must thus show some robustness against model mismatch. To get a first hint, we generated in our simulation amplitude information according to both Swerling I and III being processed according to both modelling assumptions. The results for the four possible combinations are summarized in table I. Besides the quantities already shown in Figure 9, we also listed the total energy spent for tracking (relative units).

1. For matching models, the RCS estimates are nearly bias-free and more or less roughly consistent.
2. For Swerling III fluctuations, the estimates are more accurate than in case of Swerling I.
3. For Swerling I (no mismatch), more energy is spent than for Swerling III (keeping $SN_k|_{k-1}$ constant).
4. If Swerling I amplitudes are processed according to Swerling III, the RCS is overestimated, consistency is lost.
5. It is underestimated if Swerling III amplitudes are processed according to Swerling I.
6. Mismatch does not greatly affect the performance (energy).

F. Adaptive Energy Management.

Finally we have to show up to what degree the radar energy to be spent can be reduced by estimating the RCS in comparison to worst-case assumptions. In Figure 9 the mean radar energy spent for track maintenance is displayed. The dotted lines refer to IMM-MHT tracking using the true RCS of the objects (as previously discussed). In a practical application, this cannot be realized; the resultant curves, however, may serve as a reference to discuss the performance of RCS-adaptive algorithms. The solid lines denote methods that exploit signal strength information for estimating the RCS (Worst-Case Kalman filter, IMM-MHT). Dashed lines indicate algorithms that use a worst-case assumption (here: 0.5 m², missile) on the RCS (KF, IMM-MHT).

A comparison between sensor control by using the true RCS (not available in a real application) and methods exploiting recursive RCS estimates is of particular interest. The largest deviation is observed for scenario 1 ($\bar{\sigma} = 4$ m²). This is to be expected, as the recursion was started with a worst-case assumption. The discrepancy between both curves, however, is not very significant in all four cases. Compared with IMM-MHT (Worst-Case

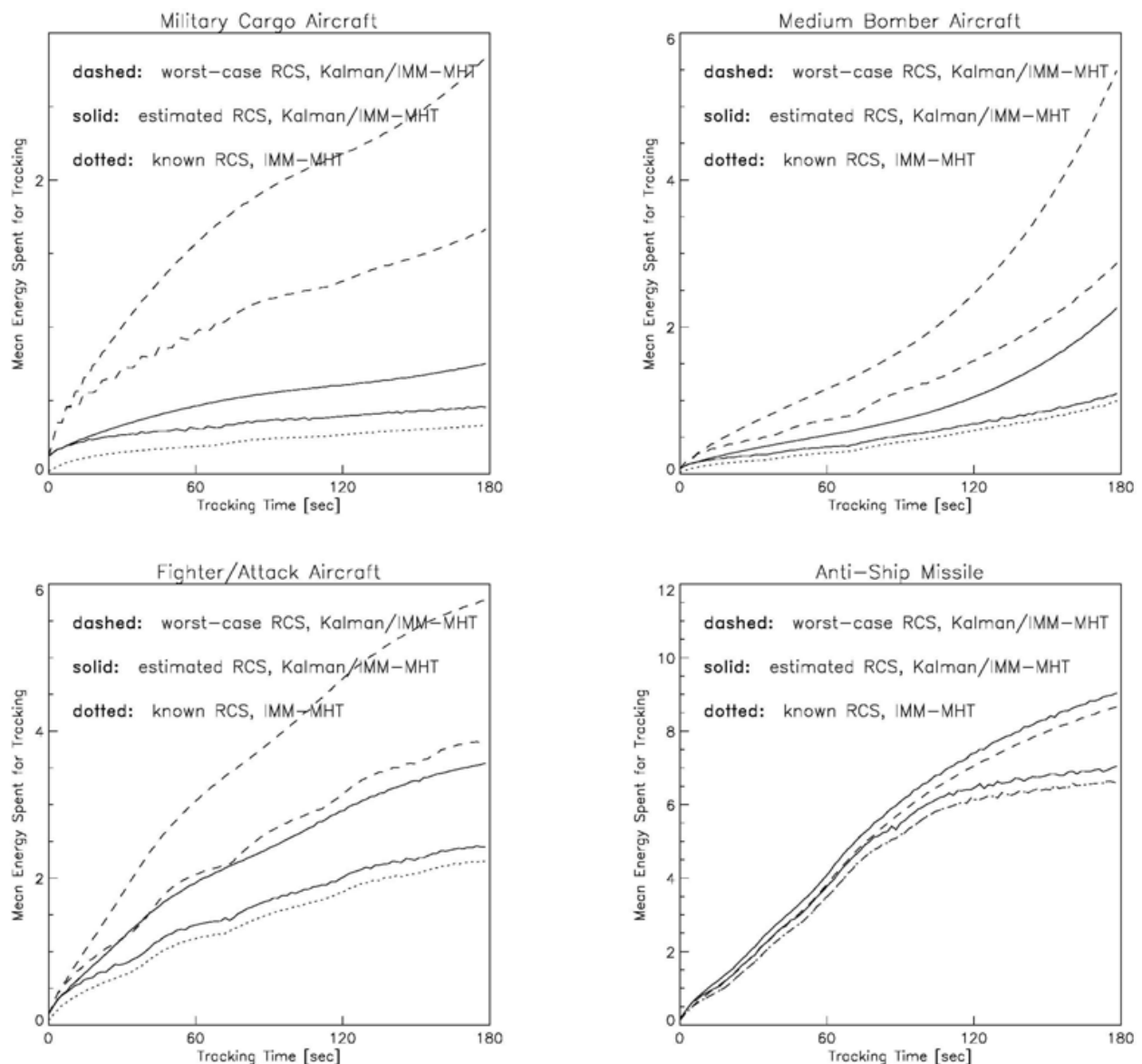


Fig. 10. Mean Number of Allocations for Different Filters and Trajectories

RCS) it can be neglected. The difference between sensor control with known and estimated RCS is roughly constant during tracking. We thus conclude that it is caused primarily in the initiation phase where not much signal strength information is yet available. As soon as reliable RCS estimates have been produced, the performance is practically identical. Figure 9 also shows how the resource savings due to adaptive dynamics models and RCS-adaptive energy management are related to each other.

In table II, scalar performance measures are summarized for all scenarios and processing methods: object revisit intervals (ΔT), sensor allocations required, energy spent for track maintenance (time averages taken over the tracking time). The last column shows the energy spent by the various methods relative to IMM-MHT with known RCS. Compared with IMM-MHT (Worst-Case RCS), the gain is: 3.8 (cargo aircraft), 2.6 (Bomber), 1.5 (Fighter), .9 (anti-ship missile). Hence, in the missile-scenario, where the worst-case assumption is correct, a small loss of performance must be taken into account.

object type	RCS	filter	ΔT [s]	revisits	energie	rel.
Cargo	worst case	Kalman	3.3	55.1	2828	8.5
		IMM-MHT	6.5	32.6	1664	5.0
	estimated	Kalman	2.0	90.3	750	2.2
		IMM-MHT	4.9	45.0	453	1.4
	known		4.9	46.4	334	1
Bomber	worst case	Kalman	3.1	60.1	5488	5.5
		IMM-MHT	6.4	34.0	2868	2.9
	estimated	Kalman	2.2	85.5	2257	2.3
		IMM-MHT	5.1	44.2	1095	1.1
	known		5.0	45.7	993	1
Fighter	worst case	Kalman	2.8	67.3	5786	2.6
		IMM-MHT	4.9	43.3	3882	1.7
	estimated	Kalman	2.2	85.6	3563	1.6
		IMM-MHT	3.9	54.0	2420	1.1
	known		3.8	55.1	2226	1
Missile	worst case	Kalman	2.1	86.6	8657	1.3
		IMM-MHT	4.1	56.1	6593	1
	estimated	Kalman	2.2	85.4	9036	1.4
		IMM-MHT	4.2	55.4	7042	1.1
	known		4.1	56.1	6593	1

Table II. Gain by rcs-adaptive energy control

5. Adaptive sensor management: summary of results

The gain by exploiting adaptive dynamics models and signal amplitude information is demonstrated by simulations with standard benchmark trajectories representative of typical military objects (cargo aircraft, medium bomber, fighter, and anti-ship missile) [8], [9]. Preliminary results were published in [25].

1. In the case of IMM-MHT, simple worst/best-case considerations seem to be sufficient for modelling the object dynamics. Medium-case models implying additional, a priori unknown parameters (e.g. transitions matrices) result in significant performance improvements only for standard IMM algorithms. IMM-MHT thus permits simplified, more *qualitative* models without significant loss of performance.

2. Compared with worst-case Kalman filtering, IMM results in considerable resource savings. The reduction with respect to the number of allocations required and the energy spent for track maintenance is roughly comparable and varies between 50 and 100% depending on the scenario considered. Essentially, the savings are due to longer revisit intervals on an average.
3. IMM-MHT improves on standard IMM algorithms. The difference, however, is less significant than between standard IMM and worst-case Kalman filtering. Besides simplified modelling assumptions, the practical use of IMM-MHT primarily consists in the exploration of the theoretical boundaries that limit the performance improvements achievable by adaptive dynamics models.
4. Due to abrupt maneuvers after a longer inertial flight, IMM-type tracking must necessarily be complemented by efficient Bayesian algorithms for adaptive beam positioning and local search. If used, however, tracking process remains highly stable, because all information on the possible dynamical behavior of the objects is taken into account.
5. By processing object amplitude information along the estimated trajectory, the a priori unknown RCS of the objects can (roughly) be estimated. The estimate is approximately bias-free; its variance corresponds with the empirical variance. It is closely related to the tracking process and might provide a contribution to object classification. Within certain limits, the method seems to be rather robust against model mismatch.
6. Compared with worst-case assumptions on the object RCS, significant energy savings can be obtained by exploiting amplitude information. Depending on the scenario considered, the gain is larger than the improvement achievable by adaptive dynamics models. The difference to algorithms that use of the correct object RCS (available in a simulation) is comparatively small and arises mainly in the initiation phase.

6. References

- [1] M. Abramowitz and I.A. Segun. *Handbook of Mathematical Functions*, Dover (1965).
- [2] Y. Bar-Shalom, X.-R. Li, and T. Kirubarajan. *Estimation with Applications to Tracking and Navigation*. Wiley & Sons, 2001.
- [3] Y. Bar-Shalom and X.-R. Li. *Estimation and Tracking: Principles, Techniques, Software*, Boston, MA: Artech House, 1993.
- [4] J. Biermann. Understanding Military Information Processing - An Approach to Support Intelligence in Defence and Security. In *NATO Advanced Research Workshop on Data Fusion Technologies in Harbour Protection*, Tallinn, Estonia, 2005.
- [5] S. Blackman. Multiple Hypothesis Methods. In *IEEE AES Magazine*, 19, 1, p. 41–52, 2004.
- [6] S. Blackman and R. Populi. *Design and Analysis of Modern Tracking Systems*. Artech House, 1999.
- [7] R. J. Dempster, S. Blackman, S. H. Roszkowski, and D. M. Sasaki. IMM/MHT Solution to Radar and Multisensor Benchmark Tracking Problems. In *SPIE 3373, Signal and Data Processing of Small objects* (1998).
- [8] W. D. Blair, G.A. Watson, T. Kirubarajan, and Y. Bar-Shalom. Benchmark for Radar Resource Allocation and Tracking objects in the Presence of ECM. In *IEEE TAES* 35, No. 4 (1998).
- [9] W. D. Blair, G. A. Watson, and K. W. Kolb. Benchmark Problem for Beam Pointing Control of Phased-Array Radar in the Presence of False Alarms and ECM. In *Proceedings 1995 American Control Conference*, Seattle WA (1994).

- [10] W. Blanding, W. Koch, and U. Nickel. Tracking Through Jamming Using 'Negative' Information. In *Proc. of the 9th International Conference on Information Fusion FUSION 2006*, Florence, Italy, July 2006. To appear also in IEEE TAES.
- [11] Philip L. Bogler. Radar Principles with Applications to Tracking Systems. John Wiley & Sons (1990).
- [12] W. Fleskes and G. van Keuk. On Single Target Tracking in Dense Clutter Environment - Quantitative Results. In *Proc. of IEE International Radar Conference RADAR 1987*, pp. 130-134.
- [13] I. S. Gradshteyn and I. M. Ryzhik. *Table of Integrals, Series, and Products*, Academic Press (1979).
- [14] D. L. Hall and J. Llinas (Eds.). *Handbook of Multisensor Data Fusion*. CRC Press, 2001.
- [15] Young-Hun Jung and Sun-Mog Hong. Modelling and Parameter Optimization of Agile Beam Radar Tracking. In IEEE TAES, vol. 39, no. 1, p.13-33, Jan. 2003.
- [16] G. van Keuk. Multihypothesis Tracking with Electronically Scanned Radar". In *IEEE AES 31*, No. 3 (1995).
- [17] G. van Keuk and S. Blackman. On Phased-Array Tracking and Parameter Control. In *IEEE AES 29*, No. 1 (1993).
- [18] T. Kirubarajan, Y. Bar-Shalom, W. D. Blair, and G. A. Watson. IMM-PDAF Solution to Benchmark for Radar Resource Allocation and Tracking Targets in the Presence of ECM", *IEEE AES 35*, No. 4 (1998).
- [19] W. Koch. A Bayesian Approach to Extended Object and Cluster Tracking using Random Matrices. In *IEEE TAES*, July 2008.
- [20] W. Koch. On Exploiting 'Negative' Sensor Evidence for object Tracking and Sensor Data Fusion. in *Information Fusion*, 8(1), 28-39, 2007.
- [21] W. Koch. Ground Target Tracking with STAP Radar: Selected Tracking Aspects. Chapter 15 in: R. Klemm (Ed.), *The Applications of Space-Time Adaptive Processing*, IEE Publishers, 2004.
- [22] W. Koch. Target Tracking. Chapter 8 in S. Stergiopoulos (Ed.), *Signal Processing Handbook*. CRC Press, 2001.
- [23] W. Koch. Fixed-Interval Retrodiction Approach to Bayesian IMM-MHT for Maneuvering Multiple Targets. In *IEEE TAES*, 36, No. 1, (2000).
- [24] W. Koch. On Adaptive Parameter Control for Phased-Array Tracking. Signal and Data Processing of Small Targets, SPIE Vol. 3809, pp. 444-455, Denver, USA, July 1999.
- [25] W. Koch and G. van Keuk. On Bayesian IMM-Tracking for Phased-Array Radar. In Proc. DGON/ITG International Radar Symposium, IRS '98, Conference Proceedings, p. 715-723, Mnchen (1998).
- [26] W. Koch and G. van Keuk. Multiple Hypothesis Track Maintenance with Possibly Unresolved Measurements. IEEE TAES, 33, No. 3 (1997).
- [27] W. Koch, J. Koller, and M. Ulmke. Ground object Tracking and Road Map Extraction. In *ISPRS Journal on Photogrammetry & Remote Sensing*, 61, 197-208, 2006.
- [28] B. F. La Scala and B. Moran. Optimal Target Tracking with Restless Bandits. In *Digital Signal Processing*, vol. 16, no. 5, p. 479-87, Sept. 2006.
- [29] B. F. La Scala, M. Rezaeian, and B. Moran. Optimal Adaptive Waveform Selection for Target Tracking. In Proc. of the 9th International Conference on Information Fusion, FUSION 2006, Florence, Italy, July 2006.

- [30] R. P. S. Mahler. "Statistics 101" for Multisensor, Multitarget Data Fusion. In *IEEE AES Magazine*, 19, 1, p. 53-64, 2004.
- [31] B. Ristic and N. Gordon. *Beyond Kalman Filtering*. Wiley, 2004.
- [32] D. Salmond. Mixture Reduction Algorithms for Target Tracking in Clutter. In *SPIE*, vol. 1305, April 1990, pp. 434-445.
- [33] P. W. Sarunic and R. J. Evans. Adaptive Update Rate Tracking using IMM Nearest Neighbour Algorithm Incorporating Rapid Re-Looks. In *IEE Proc.-Radar, Sonar, Navig.*, 144, No. 4 (1997)
- [34] R. Streit and T. E. Luginbuhl. Probabilistic Multi-Hypothesis Tracking. Naval Undersea Warfare Center Dahlgren Division, *Research Report NUWC-NPT/10/428*.
- [35] M. Wieneke and W. Koch. The PMHT: Solutions to Some of its Problems. In *Proc. of SPIE Signal and Data Processing of Small Targets*, San Diego, USA, August 2007. Also submitted to *ISIF Journal of Advances in Information Fusion*.

IntechOpen



Sensor and Data Fusion

Edited by Nada Milisavljevic

ISBN 978-3-902613-52-3

Hard cover, 436 pages

Publisher I-Tech Education and Publishing

Published online 01, February, 2009

Published in print edition February, 2009

Data fusion is a research area that is growing rapidly due to the fact that it provides means for combining pieces of information coming from different sources/sensors, resulting in ameliorated overall system performance (improved decision making, increased detection capabilities, diminished number of false alarms, improved reliability in various situations at hand) with respect to separate sensors/sources. Different data fusion methods have been developed in order to optimize the overall system output in a variety of applications for which data fusion might be useful: security (humanitarian, military), medical diagnosis, environmental monitoring, remote sensing, robotics, etc.

How to reference

In order to correctly reference this scholarly work, feel free to copy and paste the following:

Wolfgang Koch (2009). Advanced Sensor and Dynamics Models with an Application to Sensor Management, Sensor and Data Fusion, Nada Milisavljevic (Ed.), ISBN: 978-3-902613-52-3, InTech, Available from: http://www.intechopen.com/books/sensor_and_data_fusion/advanced_sensor_and_dynamics_models_with_a_n_application_to_sensor_management

INTECH
open science | open minds

InTech Europe

University Campus STeP Ri
Slavka Krautzeka 83/A
51000 Rijeka, Croatia
Phone: +385 (51) 770 447
Fax: +385 (51) 686 166
www.intechopen.com

InTech China

Unit 405, Office Block, Hotel Equatorial Shanghai
No.65, Yan An Road (West), Shanghai, 200040, China
中国上海市延安西路65号上海国际贵都大饭店办公楼405单元
Phone: +86-21-62489820
Fax: +86-21-62489821

© 2009 The Author(s). Licensee IntechOpen. This chapter is distributed under the terms of the [Creative Commons Attribution-NonCommercial-ShareAlike-3.0 License](#), which permits use, distribution and reproduction for non-commercial purposes, provided the original is properly cited and derivative works building on this content are distributed under the same license.

IntechOpen

IntechOpen